symmetry

MDPI

Review

Actual Symmetry of Symmetric Molecular Adducts in the Gas Phase, Solution and in the Solid State

Ilya G. Shenderovich

Institute of Organic Chemistry, University of Regensburg, Universitaetstrasse 31, 93053 Regensburg, Germany; Ilya.Shenderovich@ur.de

Abstract: This review discusses molecular adducts, whose composition allows a symmetric structure. Such adducts are popular model systems, as they are useful for analyzing the effect of structure on the property selected for study since they allow one to reduce the number of parameters. The main objectives of this discussion are to evaluate the influence of the surroundings on the symmetry of these adducts, steric hindrances within the adducts, competition between different noncovalent interactions responsible for stabilizing the adducts, and experimental methods that can be used to study the symmetry at different time scales. This review considers the following central binding units: hydrogen (proton), halogen (anion), metal (cation), water (hydrogen peroxide).

Keywords: hydrogen bonding; noncovalent interactions; isotope effect; cooperativity; water; organometallic complexes; NMR; DFT

Citation: Shenderovich, I.G. Actual Symmetry of Symmetric Molecular Adducts in the Gas Phase, Solution and in the Solid State. *Symmetry* **2021**, *13*, 756. https://doi.org/10.3390/sym13050756

Academic Editor: Enrico Bodo

Received: 9 April 2021
Accepted: 22 April 2021
Published: 27 April 2021

1. Introduction

If something is perfectly symmetric, it can be boring, but it cannot be wrong. If something is asymmetric, it has potential to be questioned. Note, for example, the symmetry of time in physics [1,2]. Symmetry also plays an important role in chemistry. Whether it is stereochemistry [3], soft matter self-assembly [4,5], solids [6,7], or diffusion [8], the dependence of the physical and chemical properties of a molecular system on its symmetry is often a key issue. Symmetric molecular adducts are popular model systems; they are used to analyze the effect of structure on the property chosen for research since they allow one to reduce the number of parameters [9–12]. On the other hand, symmetry in chemistry is a matter of the size and time scale in question [13]. The same molecular system can be symmetric for one experimental method and asymmetric for another. It is important to understand what processes are hidden behind this discrepancy in each specific case.

The problem of the size scale already begins at the level of the model adducts composition. What structure has the simplest model adduct with which it is possible to investigate the property under consideration? The Zundel cation ($H_5O_2^+$) and the Eigen cation ($H_9O_4^+$) seem to be the most illustrative example [14,15]. Which of these two structures is the best for simulating a hydrated proton? It seems that neither experiment nor theory can answer this question regardless of the property being discussed [16–20]. The same is valid for the hydration of the hydroxide ion [21–24]. Of course, bulk water is one of the most complex solvents in this content. The time scale problem has to do with tautomerism. For some methods, its rate is slow. In this case, experimental parameters can be observed for each of the structures presented. For other methods, this rate is fast and only average experimental parameters can be observed.

This short review discusses molecular adducts whose composition allows a symmetric structure. These adducts should be stable in organic solvents at least on the millisecond time scale. It should be possible to model the effect of the surroundings on their structure by considering the environment as a polarizable continuum. It is not limited only to the polarizable continuum model (PCM) and solvation model based on density (SMD) approximations [25–29]. It is important that the solute–solvent interactions do not have to be considered explicitly. Some examples of the molecular dynamics (MD) studies will be included as well [30–32]. If known, the symmetry of the selected adducts in the gas phase and solids is also discussed.

The main objectives of this review are to discuss (i) the influence of the environment on the symmetry of these adducts, (ii) steric hindrances caused by interactions within the adducts, (iii) competition between different noncovalent interactions responsible for stabilizing the adducts, and (iv) what experimental methods can be used to study their symmetry at different time scales. Therefore, this review is not structured according to the type of interaction that is responsible for the stabilization of the adducts, but according to the central binding unit: hydrogen (proton), halogen (anion), metal (cation), water (hydrogen peroxide).

2. Hydrogen (Proton) as the Binding Unit

Hydrogen bonding (H-bond) is one of the most important tools for controlling molecular conformation and intermolecular aggregation. A large number of potentially symmetric structures of $(AHA)^-$ and $(BHB)^+$ types is known. Here, a few of the more typical ones are discussed.

2.1. Intramolecular H-Bonds

Figure 1 shows selected molecules with an intramolecular H-bond. The lowest energy geometry of 3-carboxypropanoate (the maleate anion, Figure 1a) in the gas phase has an asymmetric H-bond. The OH and H···O distances are 1.33 and 1.10 Å [33]. However, the zero-point energy is above the energy barrier for proton transfer. Consequently, due to the motion of the mobile proton in the ground vibrational state, the H-bond is symmetric [34]. As a result, this molecule yielded a broad and featureless photoelectron spectrum [33].

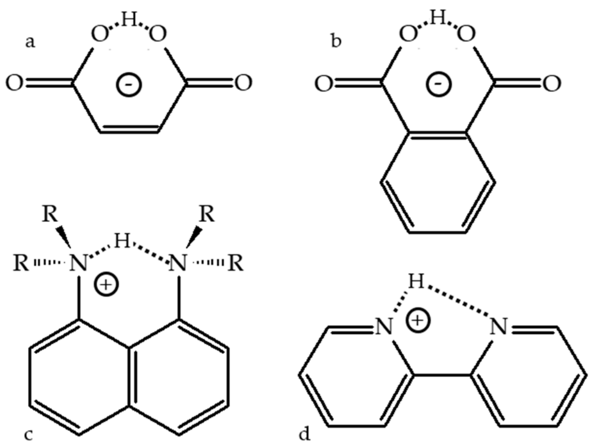

Figure 1. Potentially symmetric structures with intramolecular H-bonding. 3-carboxypropanoate (**a**), 2-carboxybenzoate (**b**), 1,8-bis(di-R-amino)-naphthalene-H^+ (**c**), 1,8-naphthyridine-H^+ (**d**).

The symmetry of the maleate anion in solution was studied using a primary H/D isotope effect on the NMR chemical shift, ${}^{P}\Delta(H/D) \equiv \delta(A\underline{D}B) - \delta(A\underline{H}B)$. The motion of the binding hydron within a H-bond should always be treated as quantum [35]. Consequently, when the mobile proton is substituted for deuteron, the geometry of the H-bond changes. For a symmetric H-bond this substitution results in a contraction of the heavy nuclei distance, that is, the strengthening of the H-bond; for an asymmetric H-bond it causes a lengthening of this distance, that is, the weakening of the H-bond [36]. These geometric changes lead to chemical shift changes. It is expected that ${}^{P}\Delta(H/D) > 0$ for symmetric H-bonds and negative for asymmetric ones (note, that other authors may define the isotope effects as $\delta(AHB) - \delta(ADB)$) [37]. For the maleate anion ${}^{P}\Delta(H/D) = 0.08$ ppm at 150 K [38] in an aprotic, highly polar CDF_3/CDF_2Cl mixture [39] and 0.03 ppm at 218 K in CD_2Cl_2 [40]. These results suggested that under these conditions this H-bond is symmetric. This conclusion was challenged by an ^{18}O-induced isotope shift [41]. This study claims that such H-bonds in solution are asymmetric due to the anisotropy of the local solvation environment [42]. This claim seems to be correct [43,44]. Chemical shift is a tensor. The discussed experiments in solution operate with the average values of the corresponding tensors. The dependence of the tensors on the H-bond geometry can be complex [45]. Although the positive sign of $^{p}\Delta(H/D)$ indicates a very strong H-bond, it does not necessarily mean that the bond is symmetric [46,47]. It would be interesting to see a detailed analysis of this effect for maleate anion. Moreover, this anion is present in solution together with a cation [48]. Their interaction can only be neglected in water due to the dissociation of the ion pair. On the other hand, the solvation of the two C=O moieties of the maleate anion by water is symmetric only on average due to a rapid change in the structure of the solvation shell caused by the thermal motion of solvent molecules. In organic solvents the anion–cation interaction cannot be neglected. It is reasonable that, with the exception of very bulky cations, it is this interaction that will determine the symmetry of the H-bond. For the bulky cations, the solute–solvent interactions become critical again. The effect of such interactions on the geometry of H-bonds should not be underestimated [49]. It is likely that at any given moment of time the H-bond in the maleate anion is asymmetric in any solvent and that its C=O moieties play an important role in this. Note that the intramolecular H-bonds of hydrogen succinate, meso-/rac-2,3-dimethylsuccinate, and (R)-(+)-methylsuccinate are asymmetric in CDF_3/CDF_2Cl [50].

Reference [51] reviews the symmetry of the H-bond of the maleate anion with different cations in the crystalline phase. Using the position of the mobile proton available from low-temperature neutron-diffraction studies on nine different hydrogen maleate salts [52–57], the authors established a correlation that allows determination of this position from X-ray diffraction (XRD) data [51,58]. There are three groups of crystals in which the deviation of the proton position from the H-bond center is below 0.06 Å, about 0.2 Å, and about 0.3 Å [51]. The symmetry of these H-bonds changes under pressure [59].

Similar results have been obtained for hydrogen phthalate, Figure 1b. Its intramolecular H-bond is symmetric in the gas phase [60]. In solution it becomes asymmetric due to solute–solvent and anion–cation interactions [60–63]. Note that the strength of this H-bond suffers from significant steric stress [64]. The energy of this bond in crystalline phthalic acid is only 9.5 kJ/mol [65] while it can be more than 100 kJ/mol for strong intermolecular H-bonds [66]. In the crystalline phase, the position of the mobile proton within the intramolecular H-bond of lithium hydrogen phthalate depends on the environment and can be both very close to the center and very asymmetric [67]. However, there does not appear to be a crystalline hydrogen phthalate with a perfectly symmetric intramolecular H-bond [68].

The symmetry of the intramolecular H-bond in 1,8-bis(dimethylamino)naphthalene-H^+ (Figure 1c) has been recently discussed in detail [69]. This molecule is the simplest representative of proton sponges, which are a certain type of aromatic diamines with unusually high basicity [70,71]. It is also the most studied molecule of this type. The intramolecular H-bond in 1,8-bis(dimethylamino)naphthalene-H^+ is strongly asymmetric in the gas phase [72] and remains asymmetric in solution [73]. The symmetry and the proton-transfer rate depend on the solvent and the anion. The more polar the solvent and the bulkier the anion, the closer the mobile proton is to the center of this H-bond [74]. The estimated residence time of the proton at a given nitrogen is about 1 picosecond [69]. In the solid state the geometry of the H-bond is asymmetric and depends on the local environment [75–77]. In general, it appears that the intramolecular H-bond in all known protonated proton sponges is asymmetric both in solution and in the solid state [78,79]. Due to the strength of the intramolecular H-bond and a slow intermolecular proton exchange in solution, proton sponges are very popular model systems for benchmark studies of spectral manifestations of H-bonding [80–86]. Alternatively, the H-bond symmetry can be purposefully lowered to investigate competing interactions [87–90].

The distance between the nitrogen atoms of 1,8-naphthyridine (2,2′-bipyridine) is too large to form a strong intramolecular H-bond, Figure 1d. In the gas phase [91], on silica surfaces [92], and in many crystals it occurs in the *trans*-configuration [93,94]. Coordination to a metal [95,96] or protonation [97] are required to stabilize the *cis*-configuration shown in Figure 1d. This *cis*-configuration of 1,8-naphthyridine-H^+ has been used to study in detail the counterion effect on intramolecular H-bonds and proton transfer using ^1H and ^{15}N NMR at 150-115 K in $CDF_3/CDClF_2$ [98]. Figure 2 shows the main results of this study. Dichloroacetic acid forms a strong intermolecular H-bond with one of the nitrogen atoms of 1,8-naphthyridine. At low temperature in the aprotic solvent this complex is stable on the millisecond time scale. The configuration of the base is unknown, but it is probably fluctuating between the *trans*- and *cis*-configurations. The position of the mobile proton depends on the current polarity of the solvent. The lower the temperature, the higher the polarity, the closer the proton is to the nitrogen atom [39]. At 115 K the geometry of this H-bond is $(N\text{-}H^+)\cdots O^-$. However, the local polarity fluctuates and causes the proton to move in the intermediate temperature range at around 120 K with a large amplitude within the H-bond. The moment the proton is at the oxygen atom, it can change the nitrogen atom with which it will be bound. Consequently, at 120 K there is an intramolecular proton exchange in the absence of the intramolecular H-bond, Figure 2a. The tetrafluoroborate anion is a weak base and it does not break the intramolecular H-bond in 1,8-naphthyridine-H^+. However, there is still a specific interaction in this anion–cation pair that makes the intramolecular proton transfer slow on the millisecond time scale, Figure 2b. Only a very bulky anion, tetrakis[3,5-bis- (trifluoromethyl)phenyl] borate, does not exhibit a preferential interaction with one of the pyridine rings. A very fast degenerate intramolecular proton transfer was detected in this case, Figure 2c. The geometry of this intramolecular H-bond was estimated to be: N-H = 1.1 Å and H⋯N = 1.7 Å [98].

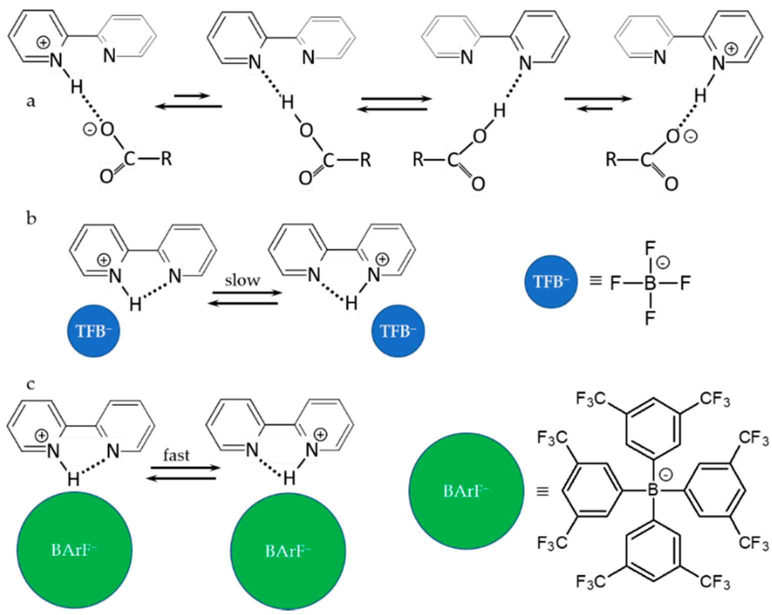

Figure 2. Anion–cation interactions, H-bonds and proton transfer in 1,8-naphthyridine-H^+ anion complexes in an aprotic polar solvent [98]. Anions: dichloroacetate (**a**), tetrafluoroborate (**b**), and tetrakis[3,5-bis- (trifluoromethyl)phenyl] borate (**c**).

2.2. Proton-Bound Homodimers

The question "What factors determine whether a proton-bound homodimer has a symmetric or an asymmetric hydrogen bond?" was answered for homodimers of the $[XHX]^+$ type in [99,100]. It was shown that the symmetry of such homodimers depends on the electronegativity of the atom X. "A more electronegative X atom tends to produce a more positively charged shared proton, which in turn facilitates the closer approach of the two X atoms and the formation of a symmetric hydrogen bond" [99]. In the gas phase, the symmetric $[X\cdots H\cdots X]^+$ homodimers are expected for X = F and, with some exceptions, O and sp-hybridized N. For X = sp^2- and sp^3-hybridized N such homodimers will be asymmetric, although proton transfer within such H-bonds can be fast. Proton-bound homodimers involving second-row atoms were studied as well [101]. Note that the calculation result can critically depend on the level of approximation [102]. High level calculations can show very good agreement with experimentally observed values [103–105].

The binding energies of such homodimers depend on the electronic properties of X. For example, there is a quadratic correlation between the binding energy and the proton affinity of X within a given set of X-R, where R is a substituent. The energy reaches its maximum at a certain value of the proton affinity [100]. This relationship is the result of a compromise between the penalty for partially deprotonating $[XH]^+$ and the benefit of partially protonating X.

In condensed matter, various noncovalent interactions compete with each other. Very specific conditions are required to observe centrosymmetric $[X\cdots H\cdots X]^+$ complexes. For example, it can be noble-gas (Ng) matrices, X = Ng [106,107]. The only complex for which the presence of a centrosymmetric structure was experimentally proved in various solvents and solids is $[F\cdots H\cdots F]^-$ [108–111]. The bond dissociation energy of $[FHF]^-$ is about 190 kJ/mol [112]. This energy is twice that of the next candidate, $[ClHCl]^-$, 100 kJ/mol [113]. It is not yet clear whether $[ClHCl]^-$, can be centrosymmetric in condensed matter [114,115]. The presence of a competing H-bond can completely break the symmetry of $[FHF]^-$ as it happens in pyridine-$H^+\cdots F^-\cdots$H-F [116].

Figure 3 shows ^{1}H, ^{2}H, and ^{19}F NMR spectra of a solution containing the $[FHF]^-$ and $[FDF]^-$ anions and the tetrabutylammonium cation in CDF_3/CDF_2Cl at 130 K [38]. For this complex $^p\Delta(H/D) \equiv \delta(F\underline{D}F) - \delta(F\underline{H}F)$ = 0.32 ppm and $^2\Delta^{19}F(D) \equiv \delta(\underline{F}D\underline{F}) - \delta(\underline{F}H\underline{F})$ = -0.37 ppm. These values were quantitatively reproduced in MP2 calculations, which confirms the centrosymmetric structure of these anions [47]. The geometry of $[FHF]^-$ in solution depends on specific interactions with solvent molecules. Molecular dynamics simulations show that in CH_2Cl_2 the main interaction is $F\cdots H$-$CHCl_2$ H-bonding, while in CCl_4 it is a weaker $F\cdots Cl$-CCl_3 halogen–halogen bonding [117]. Symmetric solvation should lead to a contraction of $[FHF]^-$ [118]. Asymmetric solvation will perturb the symmetry of $[FHF]^-$. Surprisingly, the effect can be stronger due to the halogen–halogen interactions in CCl_4 than due to the H-bonding in CH_2Cl_2 [117]. These geometric changes cannot be measured using either ^{1}H or ^{19}F NMR, because these chemical shifts are independent of the F . . . F distance at 2.3 Å [118].

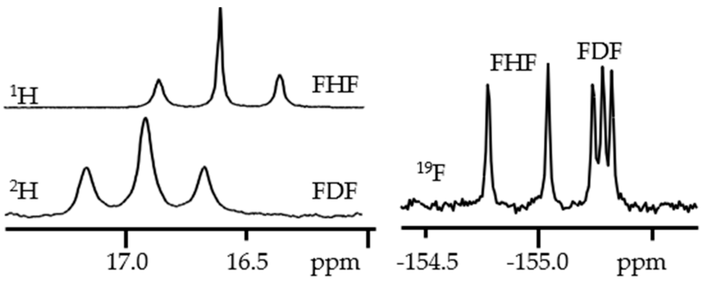

Figure 3. ^{1}H, ^{2}H, and ^{19}F NMR spectra of the $[FHF]^-$ and $[FDF]^-$ anions and the tetrabutylammonium cation in CDF_3/CDF_2Cl at 130 K [38].

$[FHF]^-$ can be centrosymmetric in solids when the environment of the fluorine atoms is symmetric [108]. The supposed examples can be found elsewhere [108,110]. Structural, energetic, and spectral properties of $[FHF]^-$ were considered in a very large number of publications. Here are just a few of the newest [119–123].

Nitrogen-containing heterocycles are probably the most experimentally studied proton-bound homodimers of the $[X\cdots H\cdots X]^+$ type. More specifically, these are symmetrically substituted pyridine derivatives. There are several reasons for this. The basicity of such derivatives can be varied over a wide range in small steps. *Ortho*-substituents can be used to protect the mobile proton from competing interactions, that extends the lifetime of such homodimers. It is easy to switch from homo- to heterodimers to study asymmetric H-bonds. The last, but not least, reason is that H-bonded complexes of pyridines are ideally suited for their NMR study, since one is not limited to ^{1}H NMR. The isotropic ^{15}N NMR chemical shift, $\delta_{iso}(^{15}N)$, of such pyridine derivatives characteristically depends on the N ... H distance [124–126]. For all of them, if $\delta_{iso}(^{15}N) \equiv 0$ in the absence of H-bonding, $\delta_{iso}(^{15}N) \approx 125$ ppm for the protonated base [127]. Due to this, for H-bonds of medium strength, the $\delta_{iso}(^{15}N)$ values can be converted to N ... H distances with high accuracy, Figure 4 [128]. This correlation has been successfully applied to measure H-bond geometries in solution [129,130], interfaces [131,132], enzyme environments [133,134], and solids [135,136].

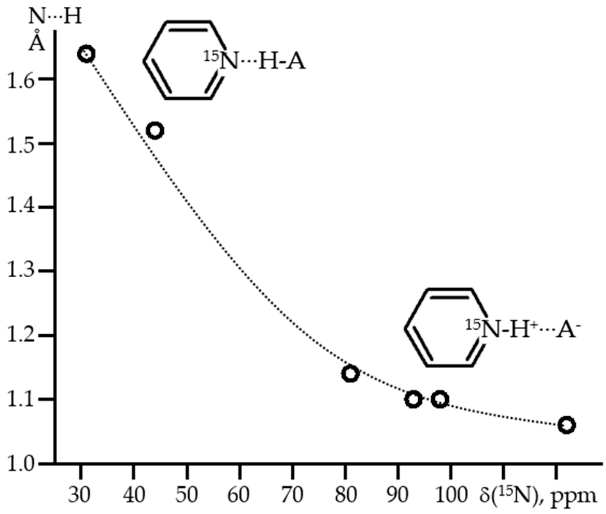

Figure 4. The average experimental N···H distances of H-bonded pyridines as a function of $\delta_{iso}(^{15}N)$ [128].

In the gas phase, the proton-bound homodimer of pyridine has an asymmetric $[N\cdots H\text{-}N]^+$ H-bond [99]. The N ... N distance is about 2.69 Å [137] and the bond dissociation energy is 105 [138] or 109 kJ/mol [139]. In solution, the N ... N distance shortens to 2.62 Å [140] and the bond dissociation energy in CD_2Cl_2 is about 15 kJ/mol [139]. The geometry of this H-bond is temperature dependent. Cooling leads to an increase in the polarity of the solvent, which causes an increase in the H-N distance and a reduction of the N···H and N...N distances.

Figure 5 shows NMR spectra of the proton-bound homodimer of pyridine in solution down to 120 K [141]. For this complex, $^{p}\Delta(H/D) = -0.95$ ppm, which unambiguously indicates the asymmetry of the H-bond, while the multiplicity of the ^{1}H and ^{15}N NMR spectra indicates a fast, reversible proton transfer within this H-bond. The observed contraction of the N ... N distance in solution is not confirmed by calculations using the polarizable continuum model (PCM [25,26]) and solvation model based on density (SMD [28]) approaches. On the contrary, these calculations predict that this distance must be about 2.75–2.77 Å [34,142]. This discrepancy was explained using the Adduct under Field (AuF) approach [143–145]. The driving force of this reversible proton transfer is a fluctuating solvation environment. The potential energy curve of this mobile proton changes from a symmetric double-well to an asymmetric single-well one. This proton tautomerism is fast on the NMR time scale that is its rate is faster than 10^3 s^{-1}. This proton transfer occurs through transition states in which the N ... N distances are shorter than in the initial $[N\cdots H\text{-}N]^+$ and the final $[N\text{-}H\cdots N]^+$ structures. As a result, the mean N ... N distance measured in NMR experiments is shorter than that of the most energetically favorable structures obtained in static calculations [146]. This proton tautomerism is slow on the electronic absorption and IR time scales [147,148]. The frequencies of the symmetric and antisymmetric CN vibrations are affected by H-bonding strong enough to discriminate between the spectral pattern of the H-bonded and protonated pyridines [148]. Consequently, the rate of this proton tautomerism is slower than 10^{11} s^{-1}.

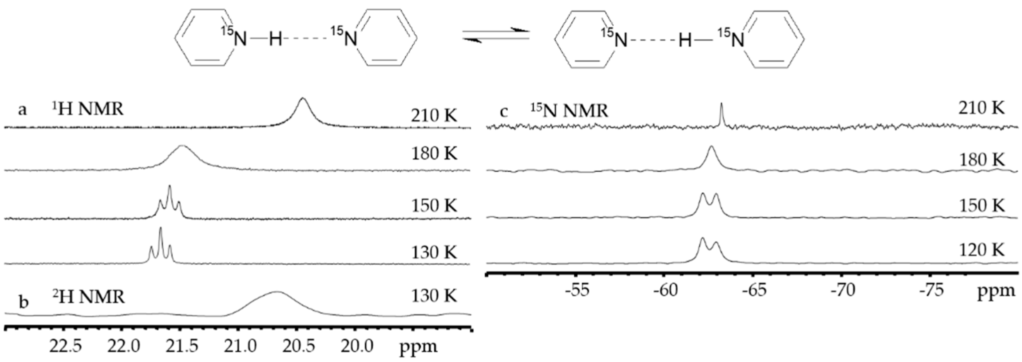

Figure 5. ^{1}H (**a**), ^{2}H (**b**), and ^{15}N (**c**) NMR spectra of [pyridine-H(D)···pyridine]$^+$ in CDF_3/CDF_2Cl at different temperatures. [141].

The geometry of the proton-bound homodimer of pyridine in the solid state depends on the counterion. In most cases, the [N···H-N]$^+$ H-bond is not linear while the sum of the N-H and H···N distances is greater than the N ... N distance of the linear H-bond in the gas phase. Generally, this sum is above 2.73 Å [149–153] while the N···H and H-N distances are 1.658 Å and 1.086 Å [154]. However, in the case of the bulky tetrakis[3,5-bis-(trifluoromethyl)phenyl] borate anion (Figure 2c), the N···H and H-N distances are 1.532 Å and 1.123 Å, thus the length of the [N···H-N]$^+$ H-bond is 2.655 Å [141]. This length is shorter than in the gas phase.

How short can be the N ... N distance in the proton-bound homodimers of pyridines? The binding energy of such homodimers will reach a maximum at a certain value of the proton affinity of the involved pyridine derivative [100]. Figure 6 shows experimental N ... N distances in the proton-bound dimers of *ortho*-unsubstituted and *ortho*-methyl substituted pyridines in CDF_3/CDF_2 at 120K as a function of calculated gas-phase proton affinities [137,140]. The N ... N distance clearly correlates with the gas-phase proton affinity. The shortest distance of 2.613 Å was observed for pyridine [140]. Steric interaction between the *ortho*-methyl groups becomes operative at the N ... N distance of ∼2.7 Å and limits the closest approach to 2.665 Å. However, this interaction is not a pure repulsion. London dispersion contributes to the binding energy of *ortho*-substituted homodimers [139,155]. As a result, the homodimers of *ortho*-substituted pyridines can be more stable than that of *ortho*-unsubstituted ones at low temperatures as long as the entropic costs are not too high. The thermodynamic parameters of a large number of the proton-bound homodimers of pyridines are available in the Supporting Information to [139].

In solution, effective proton affinities depend on solvation [156]. For example, consider derivatives of pyridine and acridine with the same gas phase proton affinity. In solution, the effective proton affinity of this acridine will be smaller than that of the pyridine derivative and the N···N distance in the proton-bound homodimer of acridine will be shorter [140]. This effect was attributed to the local ordering of the solvent molecules, which increases with the size of the solute and causes an increase in the local reaction field. The deviation from the general trend observed for halogen-substituted pyridines, **5** in Figure 6, is also probably caused by the peculiarities of the mean local surroundings. The influence of halogen–halogen interactions on molecular systems can be quite large [157,158].

Within the framework of this review, it is impossible to summarize even the main properties of carboxylic acid dimers and carboxylate-carboxylic acid dimers. These systems and their importance in practice require a special review. Cyclic dimers of carboxylic acid exhibit a rapid degenerate double proton transfer in the gas-phase [159–162], solution [163,164], and solids [165]. The binding energies of such cyclic dimers in the gas phase are about 50–70 kJ/mol [166]. In the presence of other proton acceptors, these cycles are easily opened [66,167–169]. A rapid degenerate $[O\text{-}H\cdots O]^- \rightleftharpoons [O\cdots H\text{-}O]^-$ proton transfer also occurs in carboxylate-carboxylic acid dimers [170].

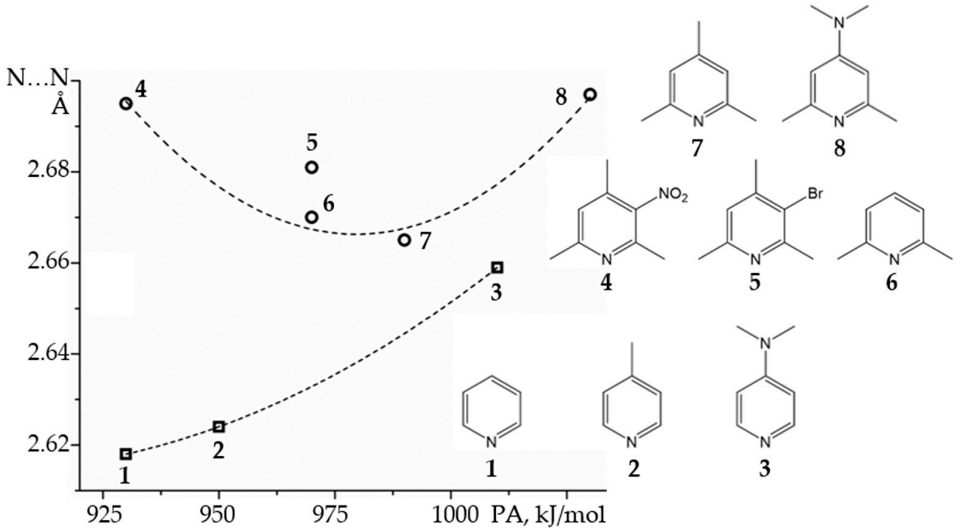

Figure 6. Experimental N … N distances in the proton-bound dimers of pyridines as a function of calculated gas-phase proton affinities (PA) [137,140]. The dotted lines are for eye guidance only.

3. Halogen (Anion) as the Binding Unit

The symmetry of halogen bound homodimers of the $[NXN]^+$ type has recently been addressed [171–173]. DFT calculations predict an asymmetric and symmetric geometries for $[N\text{-}F\cdots N]^+$ and $[N\cdots Cl\cdots N]^+$. These complexes are highly reactive, which prevents their detailed experimental study. Symmetric $[N\cdots Br\cdots N]^+$ and $[N\cdots I\cdots N]^+$ have been observed in solution [174].

The most studied type of halogen bound homodimers are $(FH)_nF^-$ complexes. These anionic clusters are ideal objects for theoretical, structural, and spectroscopic studies of H-bonding, since on the one hand they are small, and on the other hand, their geometry changes noticeably due to small external interactions or H/D isotopic substitution. There are experimental evidences that complexes $(FH)_nF^-$, where n = 2–5, can present in solution and solid state [109,175–180]. These and similar complexes have been used in theoretical studies of H-bonding binding energies [181], H-bonding with fluorine [182], vibrations of H-bonds [183,184], and NMR spin–spin coupling across H-bonds [185–192]. Of particular importance is the cooperativity (anticooperativity) of the H-bonds in these and similar complexes [193–196]. The cooperativity of H-bonds plays a very important role in biochemical reactions [197,198], molecular self-assembly [199,200], and the structure of water solvation clusters [201,202]. Only this topic will be discussed here.

Figure 7 shows ^1H, ^2H and ^{19}F NMR spectra of solutions containing $FH\cdots F^-\cdots HF$, $FH\cdots F^-\cdots DF$ and $FD\cdots F^-\cdots DF$ anions in CDF_3/CDF_2Cl at 130 K [203]. The protons of $FH\cdots F^-\cdots HF$ are located at the outer fluorine atoms. The corresponding spin–spin scalar coupling $^1J_{HF}$ = 354 Hz. The protons also couple to the central fluorine atom across the H-bonds, $^hJ_{H\cdots F} = -24$ Hz. Therefore, these protons give rise to a doublet of doublet signal, Figure 7a. The outer and central fluorine atoms couple to each other, $^{2h}J_{F\ldots F}$ = 147 Hz, and give rise to a doublet of doublet signal, Figure 7f, and a triplet of triplet signal, Figure 7d. The rate constant for proton and H-bond exchange is less than 10^3 s^{-1}. This complex is not linear, the FFF angle is about 130° [191]. There is an anti-cooperative coupling of these two H-bonds. As a result, the $FH\cdots F^-\cdots DF$ anion is asymmetric. The ^1H NMR chemical shift of the $FH\cdots F^-$ proton is larger than the ^2H NMR chemical shift of the $F^-\cdots DF$ deuteron. The former is also larger, and the latter is less than the ^1H NMR chemical shift of the protons in FH···F⁻···HF (see the arrows in Figure 7b,c). Consequently, the FH···F⁻ H-bond is shorter and the F⁻···DF one longer than the bonds in FH···F⁻···HF. This conclusion is confirmed by changes of the coupling constants and ^{19}F NMR chemical shifts. For example, in FH···F⁻···DF, for the FH···F⁻ H-bond $^{1}J_{HF}$ = 348 Hz, $^{h}J_{H\cdots F}$ = −22 Hz and $^{2h}J_{F\ldots F}$ = 151 Hz, while for the F⁻···DF H-bond $^{2h}J_{F\ldots F}$ = 140 Hz.

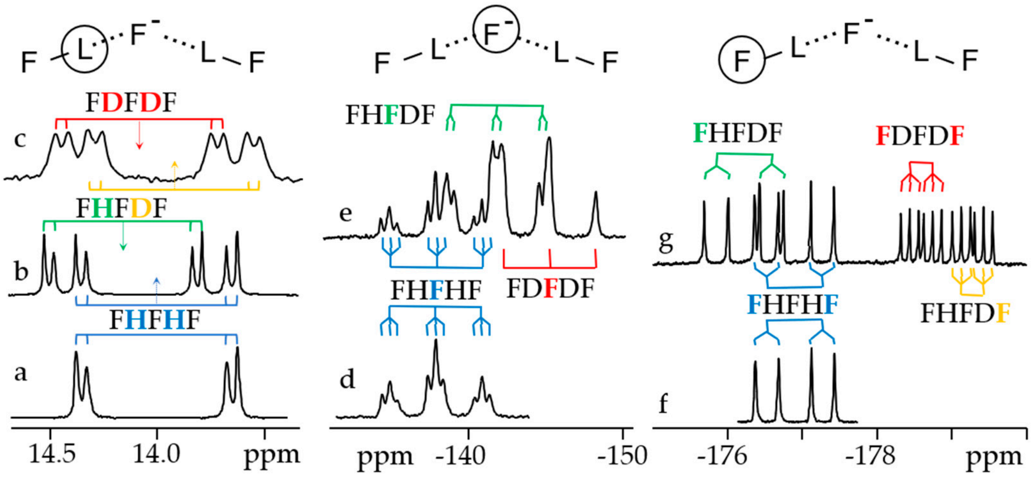

Figure 7. Experimental NMR spectra of solutions containing the FH···F⁻···HF, FH···F⁻···DF and FD···F⁻···DF anions in CDF_3/CDF_2Cl at 130 K [203]. (**a**,**b**) ^{1}H NMR, (**c**) ^{2}H NMR, (**d**–**g**) ^{19}F NMR. Arrows indicate the ^{1}H and ^{2}H NMR chemical shifts.

A detailed analysis of the experimentally obtained NMR parameters made it possible to measure the geometry of these H-bonds, Figure 8. Surprisingly, the resulting effect of the double deuteration corresponds approximately to the algebraic sum of the direct and the vicinal isotope effects [203]. These sum rules are valid for NMR parameters as well as for the F . . . F distances. For example, the midpoints of the sums of the F⁻ . . . F distances in the F-H···F⁻···D-F anion, R_{HD} = (F⁻ . . . F(H) + F⁻ . . . F(D))/2, and in the F-H···F⁻···H-F and F-D···F⁻···D-F anions, R_{HHDD} = (F⁻ . . . F(H) + F⁻ . . . F(D))/2, are shown by arrows in Figure 8. It is obvious that R_{HD} and R_{HHDD} are almost equal. The same rules are valid for the $(FH)_3F^-$ anion. There is hardly any other molecular system for which such a detailed analysis of such small effects would be possible.

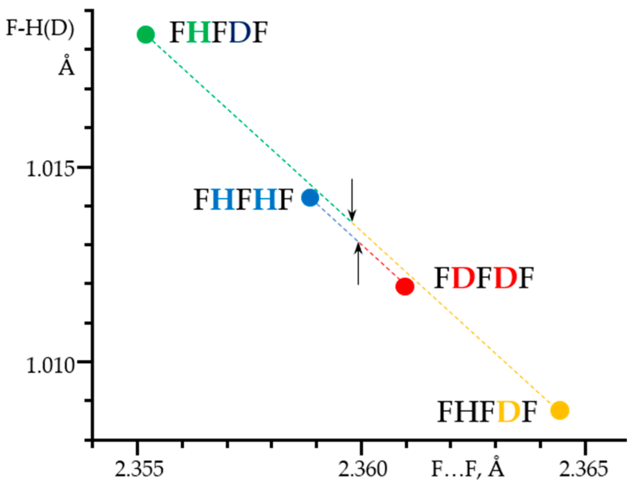

Figure 8. The F-H(D) distances in the F-H···F⁻···H-F, F-H···F⁻···D-F and F-D···F⁻···D-F anions in CDF_3/CDF_2Cl at 130 K as a function of the corresponding F . . . F distances. [203]. Arrows indicate the midpoints of the sums of the F⁻ . . . F distances in F-H···F⁻···D-F, R_{HD} = (F⁻ . . . F(H) + F⁻ . . . F(D))/2, and in F-H···F⁻···H-F and F-D···F⁻···D-F, R_{HHDD} = (F⁻ . . . F(H) + F⁻ . . . F(D))/2.

4. Metal (Cation) as the Binding Unit

Symmetric transition metal organometallics are not necessarily the most effective catalysts. However, the elucidation of their structure in solution can be greatly facilitated if they are or can be symmetric. Although ^{1}H and ^{13}C NMR are not always sufficient to determine the structure of organometallic species, ^{31}P NMR can be very useful when phosphorous is coordinated to the metal center. Only 1,3,5-triaza7-phosphaadamantane (PTA, Figure 9) complexes will be considered here. The rationale for this choice is explained as follows. The ^{31}P isotope is the only stable isotope of phosphorus. It has a spin quantum number of 1/2 and a wide chemical shift range of about 400 ppm. This nucleus is a very convenient NMR probe for studying molecular complexes [99,204–206], organometallics [207–210], and mobility at interfaces [211–213]. For example, ^{31}P NMR has been used to study the effect of temperature and hydration on the mobility of small to bulky molecules loaded onto mesoporous silica [214]. However, ^{31}P NMR shielding can depend on the conformation of the molecule [215], the crystalline electric field [216], while various noncovalent interactions can cause similar changes [217]. These disadvantages are completely absent in the case of PTA. PTA is a rigid and relatively chemically inert molecule. In acidic solution, PTA would be protonated at one of its nitrogen atoms. This protonation results in a 6 ppm change in $\delta_{iso}(^{31}P)$ [218]. In contrast, when PTA is coordinated to transition metals, its chemical shift varies in a wide range [219]. Moreover, the value of its $\delta_{iso}(^{31}P)$ in transition metal organometallics depends on the *trans*-ligand [220,221]. Therefore, ^{31}P NMR of PTA can be used to study whether the symmetry of its complexes is the same in the solid and solution phases.

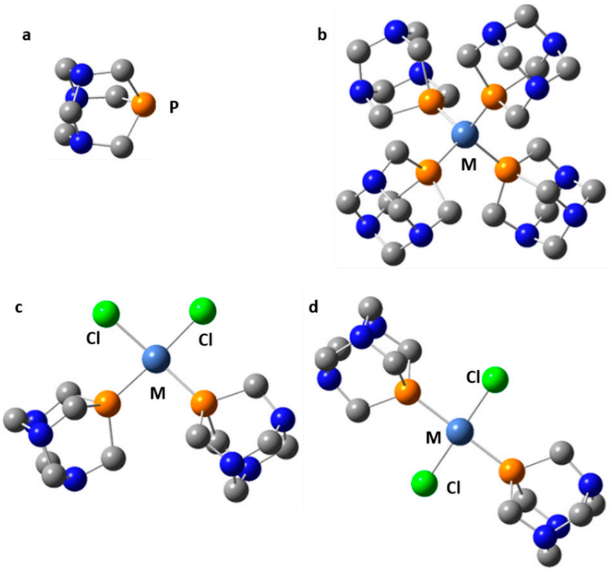

Figure 9. Selected transition metal complexes of PTA (**a**): M(PTA)$_4$ (M = Ni, Pd, Pt, Cu^{+}) (**b**), *cis*-Cl$_2$M(PTA)$_2$ (M = Ni, Pd, Pt) (**c**), *trans*-Cl$_2$M(PTA)$_2$ (M = Ni, Pd, Pt) (**d**).

Figure 9 shows three types of transition metal complexes of PTA: M(PTA)$_4$ (where M = Ni, Pd, Pt, Cu^{+}), *cis*-Cl$_2$M(PTA)$_2$ (where M = Ni, Pd, Pt) and *trans*-Cl$_2$M(PTA)$_2$ (where M = Ni, Pd, Pt). $\delta_{iso}(^{31}P)$ of PTA in these complexes were calculated under the *w*B97XD/Def2QZVP approximation [222–224] and compared to the experimental $\delta_{iso}(^{31}P)$ in solution [9], Table 1. For Ni(0)(PTA)$_4$, Pd(0)(PTA)$_4$ and Cu^{+}(I)(PTA)$_4$, the calculated values are very close to the experimental ones. A small spread in the calculated values reflects the fact that the optimized structures used in these calculations were slightly asymmetric. This flaw is not important because of the flexibility of such complexes in solution. On the contrary, the reported experimental $\delta_{iso}(^{31}P)$ for Pt(0)(PTA)$_4$ cannot correspond to this symmetric structure. The symmetry of the Cl$_2$M(II)(PTA)$_2$ complexes in solution depends on the metal. For Ni, the configuration in the crystalline state was not reported. For Pd, the configuration in the crystalline state is *cis*-$Cl_2Pd(PTA)_2$ [225]. Both the *cis*-$Cl_2Pt(PTA)_2$ and the *trans*-$Cl_2Pt(PTA)_2$ configurations are possible in the crystalline state [226,227]. According to the calculations [9], the reported experimental $\delta_{iso}(^{31}P)$ in solution correspond to the *cis*-$Cl_2Ni(PTA)_2$, *cis*-$Cl_2Pd(PTA)_2$, and *trans*-$Cl_2Pt(PTA)_2$ configurations, Table 1.

Table 1. Experimental and calculated ^{31}P NMR isotropic chemical shifts of selected transition metal complexes of PTA.

Complex	Experimental $\delta_{iso}(^{31}P)$, ppm	Calculated $\delta_{iso}(^{31}P)$, ppm [1]
PTA	−104.3 [228]	−104
$Ni(PTA)_4$	−44.8 [229],−45.7 [230]	−46; −46; −47; −47
$Pd(PTA)_4$	−56.5 [229], −58.7 [230]	−53; −56; −57; −57
$Pt(PTA)_4$	−74.5 [230]	−34; −39; −39; −39
$[NO_3]^-Cu^+(PTA)_4$	−78.2 [231]	−84; −84; −84; −85
$Cl_2Ni(PTA)_2$	−1.2 [232]	–
cis-$Cl_2Ni(PTA)_2$	–	−13; −21
trans-$Cl_2Ni(PTA)_2$	–	−36; −36
$Cl_2Pd(PTA)_2$	−21 [230], −18 [232]	–
cis-$Cl_2Pd(PTA)_2$	–	−13; −14
trans-$Cl_2Pd(PTA)_2$	–	−37; −37
$Cl_2Pt(PTA)_2$	−51 [230], −47.5 [232]	–
cis-$Cl_2Pt(PTA)_2$	–	−17; −18
trans-$Cl_2Pt(PTA)_2$	–	−46; −46

[1] Calculated under the *w*B97XD/Def2QZVP approximation, σ^{ref} = 308 ppm [9].

5. Water (Hydrogen Peroxide) as the Binding Unit

Water molecules like each other. Being adsorbed on a silica surface, water tends to self-aggregate even at concentrations below the monolayer, when many other molecules are still uniformly distributed on the surface [233–235]. In aprotic organic solvents at low concentrations, water molecules can be in a monomeric state. In this state, the ^1H NMR chemical shift of water is less than 2 ppm [236]. At higher concentrations, water molecules form clusters. In this state, their ^1H NMR chemical shift is about 4.8 ppm. The concentration at which water changes the state depend on the solvent and temperature [236]. The stronger H-bonding with the solvent and the higher the temperature, the higher the concentration at which water prefers homoclusters. At room temperature, it occurs when the water concentration is above 10–50 mM [236]. In dimethyl sulfoxide, water presents in the monomeric state at much higher concentrations. In this solvent, the ^1H NMR chemical shift of water is 3.3 ppm. Therefore, it is obvious that water is strongly H-bonded to solvent molecules. These are most likely symmetric complexes in which two solvent molecules share one water molecule. This type of complex has been observed experimentally in organic solutions at low temperatures in the presence of an excess of pyridine [237] and in frozen pyridine–water mixtures in porous materials [201]. Figure 10 shows the structure of 2:1 pyridine:water and collidine:water complexes, where collidine stands for 2,4,6-trimethylpyridine. In these complexes, the experimentally measured N···H distances are 1.82 Å for pyridine and 1.92 Å for collidine [237]. The basicity of collidine is higher than that of pyridine. Consequently, the greater distance is the result of steric interactions of the *ortho*-methyl groups in the 2:1 collidine:water complex. Indeed, in 1:n base:water complexes, where n >> 1, the experimentally measured N···H distances are 1.69 Å for pyridine and 1.64 Å for collidine. The strong shortening of the distances in both cases is the result of the anticooperative interaction of H-bonds in the 2:1 base:water complex and the cooperative interaction of H-bonds in water clusters.

Similar symmetric complexes can often be found in crystals. For example, Figure 11a shows the structure of triphenylphosphine oxide hemihydrate. In this symmetric complex the O . . . O distance is 2.91 Å [238]. There is another modification of triphenylphosphine oxide hemihydrate with two different P=O··H-O-H···O=P H-bonds with the O . . . O distances of 2.84 and 2.87 Å [239]. ^{31}P NMR study of the crystalline triphenylphosphine oxide hemihydrate demonstrated that this water is mobile at least within the borders of one structural unit [240]. Presumably, this mobility reflects a specific property of the P=O group. This group can simultaneously form two equally strong H-bonds [241]. For example, Figure 11b shows the structure of tricyclohexylphosphine oxide monohydrate [213]. These two water molecules are already immobile [217]. This H-bond network is asymmetric, with two O . . . O distances of 2.844 and two of 2.897 Å [213]. Surprisingly, water can be replaced with hydrogen peroxide. Figure 11c shows the structure of hydrogen peroxide tricyclohexylphosphine oxide [242]. This H-bond network is asymmetric as well, with two O . . . O distances of 2.743 and two of 2.771 Å. In hydrogen peroxide triphenylphosphine oxide these distances are 2.677 and 2.718 Å [243]. The decreasing distances indicate that the total energy of hydrogen peroxide H-bond networks is higher than in the case of water. This may be the reason that there are several other complexes of hydrogen peroxide with phosphine oxides of the same structure. For example, in *t*Bu_3-phosphine oxide hydrogen peroxide the O . . . O distances are 2.728 and 2.737 Å [243]. In hydrogen peroxide tris(4-methylphenyl)(oxo)-phosphine they are 2.765 and 2.774 Å [244].

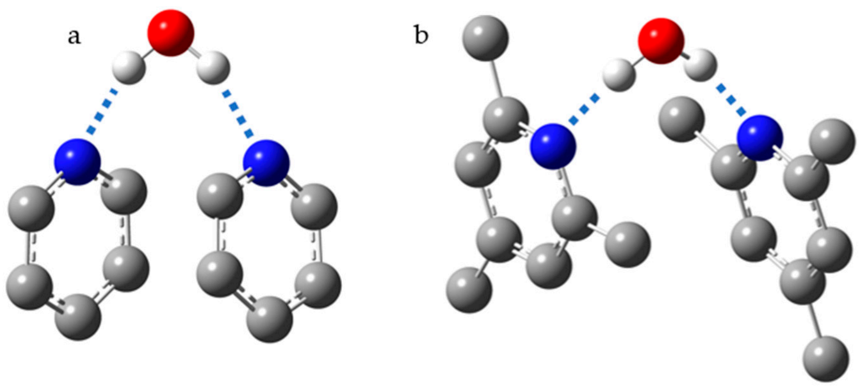

Figure 10. The most energetically favorable structures for 2:1 pyridine:water (**a**) and collidine:water (**b**) complexes.

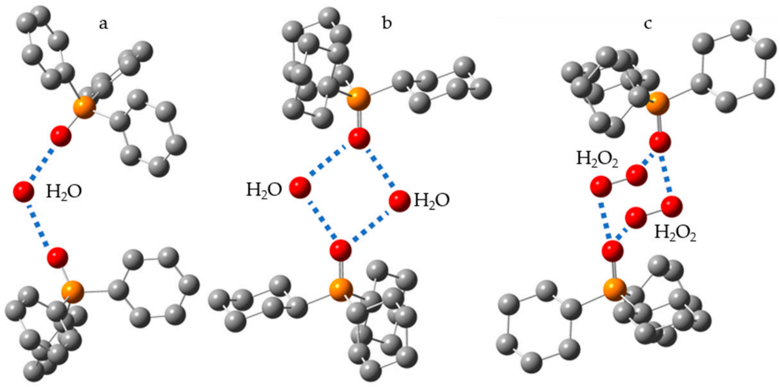

Figure 11. H-bond network structures of triphenylphosphine oxide hemihydrate (**a**), tricyclohexylphosphine oxide monohydrate (**b**), and hydrogen peroxide tricyclohexylphosphine oxide (**c**).

The NH_2 group of anilines is another example of the binding units that can initiate the formation of symmetric H-bonded molecular adducts [245–247].

6. Conclusions

The possibility of being something does not guarantee the ability to actually become that. Molecular adducts, whose composition allows a symmetric structure, can actually be symmetric, symmetric on a certain time scale, or asymmetric. Analysis of this symmetry in a given system can be used to assess its properties and interactions with the environment.

Only a few types of such molecular systems are considered in this review. These examples reflect the most important aspects of symmetric molecular adducts:

(i) Steric hindrance and structural rigidity are not the only reasons why complexes can be asymmetric in the gas phase.
(ii) At any given moment of time, the solvation shell is somewhat asymmetric.
(iii) Dynamic processes in crystalline solids can be facilitated if the initial and final states are equivalent.
(iv) The motion of the proton in a H-bond should always be treated as quantum.

The reader may find it useful to refer to other recent publications on the interactions of tetrahedral pnicogen and tetrel centres with Lewis bases [248], the coordination of triel centers [249], tetraphosphido complexes [250], dinuclear metal hydride complexes [251], crystalline peroxosolvates [252], the self-association of phosphonic acids [253], intramolecular H-bond dynamics [254], and a consistent description of noncovalent interactions [255].

Funding: This research received no external funding.

Institutional Review Board Statement: Not applicable.

Informed Consent Statement: Not applicable.

Data Availability Statement: Data sharing is not applicable to this article.

Conflicts of Interest: The author declares no conflict of interest.

References

1. Mehlberg, H. Time, Causality, and the Quantum Theory. In *Studies in the Philosophy of Science*; Fawcett, C.R., Cohen, R.S., Eds.; Springer: Berlin/Heidelberg, Germany, 1980.
2. Leifer, M.S.; Pusey, M.F. Is a time symmetric interpretation of quantum theory possible without retrocausality? *Proc. R. Soc. A* **2017**, *473*, 20160607. [CrossRef] [PubMed]
3. Castilla, A.M.; Ramsay, W.J.; Nitschke, J.R. Stereochemistry in Subcomponent Self-Assembly. *Acc. Chem. Res.* **2014**, *47*, 2063–2073. [CrossRef] [PubMed]
4. Wang, Y.-L.; Li, B.; Sarman, S.; Mocci, F.; Lu, Z.-Y.; Yuan, J.; Laaksonen, A.; Fayer, M.D. Microstructural and Dynamical Heterogeneities in Ionic Liquids. *Chem. Rev.* **2020**, *120*, 5798–5877. [CrossRef] [PubMed]
5. Wang, Y.; Wang, Y.; Breed, D.; Manoharan, V.N.; Feng, L.; Hollingsworth, A.D.; Weck, M.; Pineet, D.J. Colloids with valence and specific directional bonding. *Nature* **2012**, *491*, 51–55. [CrossRef]
6. Ungur, L.; Le Roy, J.J.; Korobkov, I.; Murugesu, M.; Chibotaru, L.F. Fine-tuning the Local Symmetry to Attain Record Blocking Temperature and Magnetic Remanence in a Single-Ion Magnet. *Angew. Chem. Int. Ed.* **2014**, *53*, 4413–4417. [CrossRef]
7. Sun, W.-B.; Yan, P.-F.; Jiang, S.-D.; Wang, B.-W.; Zhang, Y.-Q.; Li, H.-F.; Chen, P.; Wang, Z.-M.; Gao, S. High symmetry or low symmetry, that is the question—high performance Dy(iii) single-ion magnets by electrostatic potential design. *Chem. Sci.* **2016**, *7*, 684–691. [CrossRef]
8. Peng, J.; Cao, D.; He, Z.; Guo, J.; Hapala, P.; Ma, R.; Cheng, B.; Chen, J.; Xie, W.J.; Li, X.-Z.; et al. The effect of hydration number on the interfacial transport of sodium ions. *Nature* **2018**, *557*, 701–705. [CrossRef]
9. Shenderovich, I.G. 1,3,5-Triaza-7-Phosphaadamantane (PTA) as a ^{31}P NMR Probe for Organometallic Transition Metal Complexes in Solution. *Molecules* **2021**, *26*, 1390. [CrossRef]
10. Grabowski, S.J. Hydrogen Bond and Other Lewis Acid–Lewis Base Interactions as Preliminary Stages of Chemical Reactions. *Molecules* **2020**, *25*, 4668. [CrossRef]
11. Grabowski, S.J.; Ugalde, J.M.; Andrada, D.M.; Frenking, G. Comparison of Hydrogen and Gold Bonding in $[XHX]^-$, $[XAuX]^-$, and Isoelectronic $[NgHNg]^+$, $[NgAuNg]^+$ (X=Halogen, Ng=Noble Gas). *Chem. Eur. J.* **2016**, *22*, 11317–11328. [CrossRef]
12. Alkorta, I.; Elguero, J. Review on DFT and ab initio Calculations of Scalar Coupling Constants. *Int. J. Mol. Sci.* **2003**, *4*, 64–92. [CrossRef]
13. Kellman, M.E. Symmetry in chemistry from the hydrogen atom to proteins. *Proc. Natl. Acad. Sci. USA* **1996**, *93*, 14287–14294. [CrossRef] [PubMed]
14. Zundel, G.; Metzger, H. Energiebänder der tunnelnden Überschuß-Protonen in flüssigen Säuren. Eine IR-spektroskopische Untersuchung der Natur der Gruppierungen $H_5O_2^+$. *Z. Phys. Chem.* **1968**, *58*, 225–245. [CrossRef]
15. Wicke, E.; Eigen, M.; Ackermann, T. Über den Zustand des Protons (Hydroniumions) in wäßriger Lösung. *Z. Phys. Chem.* **1954**, *1*, 340–364. [CrossRef]
16. Carpenter, W.B.; Yu, Q.; Hack, J.H.; Dereka, B.; Bowman, J.M.; Tokmakoff, A. Decoding the 2D IR spectrum of the aqueous proton with high-level VSCF/VCI calculations. *J. Chem. Phys.* **2020**, *153*, 124506. [CrossRef]

17. Wang, E.; Zhu, B.; Gao, Y. Discontinuous transition between Zundel and Eigen for $H_5O_2^+$. *Chin. Phys. B* **2020**, *29*, 083101. [CrossRef]
18. Li, C.; Swanson, J.M.J. Understanding and Tracking the Excess Proton in Ab Initio Simulations; Insights from IR Spectra. *J. Phys. Chem. B* **2020**, *124*, 5696–5708. [CrossRef]
19. Vener, M.V.; Kong, S.; Levina, A.A.; Shenderovich, I.G. Spectroscopic Signatures of $[H_9O_4]^+$ and $[H_{13}O_6]^+$ Ions in a Polar Aprotic Environment Revealed under DFT-PCM Approximation. *Acta Chim. Slov.* **2011**, *58*, 402–410. [PubMed]
20. Vener, M.V.; Librovich, N.B. The structure and vibrational spectra of proton hydrates: $H_5O_2^+$ as a simplest stable ion. *Int. Rev. Phys. Chem.* **2009**, *28*, 407–434. [CrossRef]
21. Shi, H.; Gong, L.-D.; Liu, C.; Lu, L.-N.; Yang, Z.-Z. ABEEM/MM OH^- Models for $OH^-(H_2O)_n$ Clusters and Aqueous OH^-: Structures, Charge Distributions, and Binding Energies. *J. Phys. Chem. A* **2020**, *124*, 5963–5978. [CrossRef] [PubMed]
22. Herbert, J.M. Fantasy versus reality in fragment-based quantum chemistry. *J. Chem. Phys.* **2019**, *151*, 170901. [CrossRef]
23. Vener, M.V.; Shenderovich, I.G.; Rykounov, A.A. A qualitative study of the effect of a counterion and polar environment on the structure and spectroscopic signatures of a hydrated hydroxyl anion. *Theor. Chem. Acc.* **2013**, *132*, 1361. [CrossRef]
24. Librovich, N.B.; Sakun, V.P.; Sokolov, N.D. H^+ and OH^- ions in aqueous solutions vibrational spectra of hydrates. *Chem. Phys.* **1979**, *39*, 351–366. [CrossRef]
25. Cossi, M.; Barone, V.; Cammi, R.; Tomasi, J. Ab initio study of solvated molecules: A new implementation of the polarizable continuum model. *Chem. Phys. Lett.* **1996**, *255*, 327–335. [CrossRef]
26. Tomasi, J.; Mennucci, B.; Cammi, R. Quantum mechanical continuum solvation models. *Chem. Rev.* **2005**, *105*, 2999–3093. [CrossRef]
27. Scalmani, G.; Frisch, M.J. Continuous surface charge polarizable continuum models of solvation. I. General formalism. *J. Chem. Phys.* **2010**, *132*, 114110. [CrossRef] [PubMed]
28. Marenich, A.V.; Cramer, C.J.; Truhlar, D.G. Universal solvation model based on solute electron density and on a continuum model of the solvent defined by the bulk dielectric constant and atomic surface tensions. *J. Phys. Chem. B* **2009**, *113*, 6378–6396. [CrossRef]
29. Winget, P.; Dolney, D.M.; Giesen, D.J.; Cramer, C.J.; Truhlar, D.G. Minnesota Solvent Descriptor Database. Available online: http://comp.chem.umn.edu/solvation/mnsddb.pdf (accessed on 26 April 2021).
30. Onufriev, O. Implicit solvent models in molecular dynamics simulations: A brief overview. *Annu. Rep. Comput. Chem.* **2008**, *4*, 125–137. [CrossRef]
31. Orozco, M.; Luque, F.J. Theoretical methods for the description of the solvent effect in biomolecular systems. *Chem. Rev.* **2000**, *100*, 4187–4225. [CrossRef]
32. Pylaeva, S.; Allolio, C.; Koeppe, B.; Denisov, G.S.; Limbach, H.-H.; Sebastiani, D.; Tolstoy, P.M. Proton transfer in a short hydrogen bond caused by solvation shell fluctuations: An ab initio MD and NMR/UV study of an (OHO)−bonded system. *Phys. Chem. Chem. Phys.* **2015**, *17*, 4634–4644. [CrossRef]
33. Woo, H.-K.; Wang, X.-B.; Wang, L.-S.; Lau, K.-C. Probing the Low-Barrier Hydrogen Bond in Hydrogen Maleate in the Gas Phase: A Photoelectron Spectroscopy and ab Initio Study. *J. Phys. Chem. A* **2005**, *109*, 10633–10637. [CrossRef]
34. Garcia-Viloca, M.; González-Lafont, A.; Lluch, J.M. Theoretical Study of the Low-Barrier Hydrogen Bond in the Hydrogen Maleate Anion in the Gas Phase. Comparison with Normal Hydrogen Bonds. *J. Am. Chem. Soc.* **1997**, *119*, 1081–1086. [CrossRef]
35. Kiefer, P.M.; Hynes, J.T. Theoretical aspects of tunneling protontransfer reactions in a polar environment. *J. Phys. Org. Chem.* **2010**, *23*, 632–646. [CrossRef]
36. Limbach, H.-H.; Tolstoy, P.M.; Pérez-Hernández, N.; Guo, J.; Shenderovich, I.G.; Denisov, G.S. OHO Hydrogen Bond Geometries and NMR Chemical Shifts: From Equilibrium Structures to Geometric H/D Isotope Effects, with Applications for Water, Protonated Water, and Compressed Ice. *Isr. J. Chem.* **2009**, *49*, 199–216. [CrossRef]
37. Vener, M.V. Model study of the primary H/D isotope effects on the NMR chemical shift in strong hydrogen-bonded systems. *Chem. Phys.* **1992**, *166*, 311–316. [CrossRef]
38. Schah-Mohammedi, P.; Shenderovich, I.G.; Detering, C.; Limbach, H.-H.; Tolstoy, P.M.; Smirnov, S.N.; Denisov, G.S.; Golubev, N.S. H/D-Isotope Effects on NMR Chemical Shifts and Symmetry of Homoconjugated Hydrogen-Bonded Ions in Polar Solution. *J. Am. Chem. Soc.* **2000**, *122*, 12878–12879. [CrossRef]
39. Shenderovich, I.G.; Burtsev, I.G.; Denisov, G.S.; Golubev, N.S.; Limbach, H.-H. Influence of the Temperature-Dependent Dielectric Constant on the H/D Isotope Effects on the NMR Chemical Shifts and the Hydrogen Bond Geometry of Collidine-HF Complex in $CDF_3/CDClF_2$ Solution. *Magn. Reson. Chem.* **2001**, *39*, S91–S99. [CrossRef]
40. Gunnarsson, G.; Wennerström, H.; Egan, W.; Forsén, S. Proton and deuterium NMR of hydrogen bonds: Relationship between isotope effects and the hydrogen bond potential. *Chem. Phys. Lett.* **1976**, *38*, 96–99. [CrossRef]
41. Perrin, C.L.; Nielson, J.B. Asymmetry of Hydrogen Bonds in Solutions of Monoanions of Dicarboxylic Acids. *J. Am. Chem. Soc.* **1997**, *119*, 12734–12741. [CrossRef]
42. Perrin, C.L. Are Short, Low-Barrier Hydrogen Bonds Unusually Strong? *Acc. Chem. Res.* **2010**, *43*, 1550–1557. [CrossRef]
43. Mavri, J.; Hodošček, M.; Hadži, D. Ab initio SCF and Møller-Plesset calculations on the hydrogen bond in hydrogen malonate: Effects of neighbour ions and polarizable medium. *J. Mol. Struct.* **1990**, *209*, 421–431. [CrossRef]
44. Mavri, J.; Hadži, D. Influence of solvation on the hydrogen bond in hydrogen malonate an ab initio and semiempirical study. *J. Mol. Struct. Theor. Chem.* **1998**, *432*, 257–262. [CrossRef]

45. Shenderovich, I.G. Solid State NMR for Nonexperts: An overview of simple but general practical methods. *Solids* **2021**, *2*, 139–154. [CrossRef]
46. Golubev, N.S.; Detering, C.; Smirnov, S.N.; Shenderovich, I.G.; Denisov, G.S.; Limbach, H.-H.; Tolstoy, P.M. H/D Isotope Effects on NMR Chemical Shifts of Nuclei Involved in a Hydrogen Bridge of Hydrogen Isocyanide Complexes with Fluoride Anion. *Phys. Chem. Chem. Phys.* **2009**, *11*, 5154–5159. [CrossRef] [PubMed]
47. Golubev, N.S.; Melikova, S.M.; Shchepkin, D.N.; Shenderovich, I.G.; Tolstoy, P.M.; Denisov, G.S. Interpretation of H/D Isotope Effects on NMR Chemical Shifts of $[FHF]^-$ Ion Based on Calculations of Nuclear Magnetic Shielding Tensor Surface. *Z. Phys. Chem.* **2003**, *217*, 1549–1563. [CrossRef]
48. Di Muzio, S.; Ramondo, F.; Gontrani, L.; Ferella, F.; Nardone, M.; Benassi, P. Choline Hydrogen Dicarboxylate Ionic Liquids by X-ray Scattering, Vibrational Spectroscopy and Molecular Dynamics: H-Fumarate and H-Maleate and Their Conformations. *Molecules* **2020**, *25*, 4990. [CrossRef]
49. Shenderovich, I.G. Simplified Calculation Approaches Designed to Reproduce the Geometry of Hydrogen Bonds in Molecular Complexes in Aprotic Solvents. *J. Chem. Phys.* **2018**, *148*, 124313. [CrossRef] [PubMed]
50. Guo, J.; Tolstoy, P.M.; Koeppe, B.; Denisov, G.S.; Limbach, H.-H. NMR Study of Conformational Exchange and Double-Well Proton Potential in Intramolecular Hydrogen Bonds in Monoanions of Succinic Acid and Derivatives. *J. Phys. Chem. A* **2011**, *115*, 9828–9836. [CrossRef]
51. Malaspina, L.A.; Edwards, A.J.; Woińska, M.; Jayatilaka, D.; Turner, M.J.; Price, J.R.; Herbst-Irmer, R.; Sugimoto, K.; Nishibori, E.; Grabowsky, S. Predicting the Position of the Hydrogen Atom in the Short Intramolecular Hydrogen Bond of the Hydrogen Maleate Anion from Geometric Correlations. *Cryst. Growth Des.* **2017**, *17*, 3812–3825. [CrossRef]
52. Hussain, M.S.; Schlemper, E.; Fair, C. Neutron diffraction study of deuterated imidazolium hydrogen maleate: An evaluation of isotope effect on the hydrogen-bond length. *Acta Crystallogr. Sect. B Struct. Crystallogr. Cryst. Chem.* **1980**, *36*, 1104–1108. [CrossRef]
53. Hsu, B.; Schlemper, E. X−N deformation density studies of the hydrogen maleate ion and the imidazolium ion. *Acta Crystallogr. Sect. B Struct. Crystallogr. Cryst. Chem.* **1980**, *36*, 3017–3023. [CrossRef]
54. Olovsson, G.; Olovsson, I.; Lehmann, M.S. Neutron diffraction study of sodium hydrogen maleate trihydrate, $NaH[C_4H_2O_4].3H_2O$, at 120 K. *Acta Crystallogr. Sect. C Cryst. Struct. Commun.* **1984**, *40*, 1521–1526. [CrossRef]
55. Vanhouteghem, F.; Lenstra, A.; Schweiss, P. Magnesium bis (hydrogen maleate) hexahydrate, $[Mg(C_4H_3O_4)_2].6H_2O$, studied by elastic neutron diffraction and ab initio calculations. *Acta Crystallogr. Sect. B Struct. Sci.* **1987**, *43*, 523–528. [CrossRef]
56. Sequeira, A.; Rajagopal, H.; Gupta, M.; Vanhouteghem, F.; Lenstra, A.; Geise, H. Tetraaquabis (hydrogen maleato) zinc (II) by neutron diffraction and tetraaquabis (hydrogen maleato) nickel (II) by high-order X-ray diffraction. *Acta Crystallogr. Sect. C Cryst. Struct. Commun.* **1992**, *48*, 1192–1197. [CrossRef]
57. Madsen, D.; Flensburg, C.; Larsen, S. Properties of the experimental crystal charge density of methylammonium hydrogen maleate. A salt with a very short intramolecular O-H-O hydrogen bond. *J. Phys. Chem. A* **1998**, *102*, 2177–2188. [CrossRef]
58. Malaspina, L.A.; Hoser, A.A.; Edwards, A.J.; Woińska, M.; Turner, M.J.; Price, J.R.; Sugimoto, K.; Nishibori, E.; Bürgi, H.-B.; Jayatilaka, D.; et al. Hydrogen atoms in bridging positions from quantum crystallographic refinements: Influence of hydrogen atom displacement parameters on geometry and electron density. *CrystEngComm* **2020**, *22*, 4778. [CrossRef]
59. Poręba, T.; Macchi, P.; Casati, N. Structural Variety of Alkali Hydrogen Maleates at High Pressure. *Cryst. Growth Des.* **2020**, *20*, 4375–4386. [CrossRef]
60. Garcia-Viloca, M.; González-Lafont, A.; Lluch, J.M. Asymmetry of the Hydrogen Bond of Hydrogen Phthalate Anion in Solution. A QM/MM Study. *J. Am. Chem. Soc.* **1999**, *121*, 9198–9207. [CrossRef]
61. Perrin, C.L.; Lau, J.S. Hydrogen-Bond Symmetry in Zwitterionic Phthalate Anions: Symmetry Breaking by Solvation. *J. Am. Chem. Soc.* **2006**, *128*, 11820–11824. [CrossRef]
62. Perrin, C.L. Symmetry of hydrogen bonds in solution. *Pure Appl. Chem.* **2009**, *81*, 571–583. [CrossRef]
63. Mori, Y.; Masuda, Y. Effect of solvent on proton location and dynamic behavior in short intramolecular hydrogen bonds studied by molecular dynamics simulations and NMR experiments. *Chem. Phys.* **2015**, *458*, 18–29. [CrossRef]
64. Jóźwiak, K.; Jezierska, A.; Panek, J.J.; Goremychkin, E.A.; Tolstoy, P.M.; Shenderovich, I.G.; Filarowski, A. Inter- vs. Intramolecular Hydrogen Bond Patterns and Proton Dynamics in Nitrophthalic Acid Associates. *Molecules* **2020**, *25*, 4720. [CrossRef] [PubMed]
65. Zhurov, V.V.; Pinkerton, A.A. Quantifying the Inter- and Intramolecular Interactions in Crystalline Phthalic Acid. *Cryst. Growth Des.* **2014**, *14*, 5685–5691. [CrossRef]
66. Borissova, A.O.; Lyssenko, K.A.; Gurinov, A.A.; Shenderovich, I.G. Energy Analysis of Competing Non-Covalent Interaction in 1:1 and 1:2 Adducts of Collidine with Benzoic Acids by Means of X-Ray Diffraction. *Z. Phys. Chem.* **2013**, *227*, 775–790. [CrossRef]
67. Küppers, H.; Takusagawa, F.; Koetzle, T.F. Neutron diffraction study of lithium hydrogen phthalate monohydrate: A material with two very short intramolecular O···H···O hydrogen bonds. *J. Chem. Phys.* **1985**, *82*, 5636. [CrossRef]
68. Langkilde, A.; Madsen, D.; Larsen, S. Structures of three salts of phthalic acid; variation in crystal packing and geometry of the hydrogen phthalate ion. *Acta Crystallogr. Sect. B Struct. Sci.* **2004**, *60*, 502–511. [CrossRef] [PubMed]
69. Piękoś, P.; Jezierska, A.; Panek, J.J.; Goremychkin, E.A.; Pozharskii, A.F.; Antonov, A.S.; Tolstoy, P.M.; Filarowski, A. Symmetry/Asymmetry of the NHN Hydrogen Bond in Protonated 1,8-Bis(dimethylamino)naphthalene. *Symmetry* **2020**, *12*, 1924. [CrossRef]

70. Alder, R.W.; Bowman, P.S.; Steele, W.R.; Winterman, D.R. The remarkable basicity of 1,8-bis(dimethylamino)naphthalene. *Chem. Commun.* **1968**, 723–724. [CrossRef]
71. Pozharskii, A.F. Naphthalene "Proton Sponges". *Russ. Chem. Rev.* **1998**, *67*, 1–27. [CrossRef]
72. Alkorta, I.; Elguero, J. Basicity and Proton Transfer in Proton Sponges and Related Compounds: An Ab Initio Study. *Struct. Chem.* **2000**, *11*, 335–340. [CrossRef]
73. Perrin, C.L.; Ohta, B.K. Symmetry of N−H−N Hydrogen Bonds in 1,8-Bis(dimethylamino)naphthalene·H^+ and 2,7-Dimethoxy-1,8-bis(dimethylamino)naphthalene·H^+. *J. Am. Chem. Soc.* **2001**, *123*, 6520–6526. [CrossRef]
74. Pietrzak, M.; Wehling, J.P.; Kong, S.; Tolstoy, P.M.; Shenderovich, I.G.; Lopez, C.; Claramunt, R.M.; Elguero, J.; Denisov, G.S.; Limbach, H.-H. Symmetrization of Cationic Hydrogen Bridges of Protonated Sponges Induced by Solvent and Counteranion Interactions as Revealed by NMR Spectroscopy. *Chem. Eur. J.* **2010**, *16*, 1679–1690. [CrossRef]
75. Jones, A.O.F.; Kallay, A.A.; Lloyd, H.; McIntyre, G.J.; Wilson, C.C.; Thomas, L.H. The Effect of Local Crystalline Environment on Hydrogen Atom Behavior in Molecular Complexes of a Proton Sponge. *Cryst. Growth Des.* **2016**, *16*, 2123–2129. [CrossRef]
76. Lopez, C.; Lorente, P.; Claramunt, R.M.; Marin, J.; Foces-Foces, C.; Llamas-Saiz, A.L.; Elguero, J.; Limbach, H.H. Localization of Hydrogen Bond Deuterons in Proton Sponges by Dipolar Solid State ^{15}N NMR Spectroscopy. *Ber. Bunsenges. Phys. Chem. Chem. Phys.* **1998**, *102*, 414–418. [CrossRef]
77. Woźniak, K.; Wilson, C.C.; Knight, K.S.; Jones, W.; Grech, E. Neutron Diffraction of a Complex of 1,8-Bis(dimethylamino)naphthalene with 1,2-Dichloromaleic Acid. *Acta Crystallogr. Sect. B Struct. Crystallogr. Cryst. Chem.* **1996**, *52*, 691–696. [CrossRef]
78. Llamas-Saiz, A.L.; Foces-Foces, C.; Elguero, J. Proton sponges. *J. Mol. Struct.* **1994**, *328*, 297–323. [CrossRef]
79. Sobczyk, L. The specificity of the $[NHN]^+$ hydrogen bonds in protonated naphthalene proton sponges. *J. Mol. Struct.* **2010**, *972*, 59–63. [CrossRef]
80. Zhou, S.; Wang, L. Symmetry and ^1H NMR chemical shifts of short hydrogen bonds: Impact of electronic and nuclear quantum effects. *Phys. Chem. Chem. Phys.* **2020**, *22*, 4884–4895. [CrossRef] [PubMed]
81. Chmielewski, P.; Ozeryanskii, V.A.; Sobczyk, L.; Pozharskii, A.F. Primary $^1H/^2H$ isotope effect in the NMR chemical shift of $HClO_4$ salts of 1,8-bis(dimethylamino)naphthalene derivatives. *J. Phys. Org. Chem.* **2007**, *20*, 643–648. [CrossRef]
82. White, P.B.; Hong, M. ^{15}N and ^1H Solid-State NMR Investigation of a Canonical Low-Barrier Hydrogen-Bond Compound: 1,8-Bis(dimethylamino)naphthalene. *J. Phys. Chem. B* **2015**, *119*, 11581–11589. [CrossRef]
83. Gregorovic, A.; Apih, T.; Zagara, V.; Seliger, J. ^{14}N NQR spectroscopy reveals the proton position in N–H N bonds: A case study with proton sponges. *Phys. Chem. Chem. Phys.* **2019**, *21*, 306–313. [CrossRef]
84. Degtyarev, A.V.; Ryabtsova, O.V.; Pozharskii, A.F.; Ozeryanskii, V.A.; Starikova, Z.A.; Sobczyk, L.; Filarowski, A. 2,7-disubstituted proton sponges as borderline systems for investigating barrier-free intramolecular hydrogen bonds. Protonated 2,7-bis(trimethylsilyl)- and 2,7-di(hydroxymethyl)-1,8-bis(dimethylamino)naphthalenes. *Tetrahedron* **2008**, *64*, 6209–6214. [CrossRef]
85. Del Bene, J.E.; Alkorta, I.; Elguero, J. Spin-spin coupling across intramolecular N-H^+-N hydrogen bonds in models for proton sponges: An ab initio investigation. *Magn. Reson. Chem.* **2008**, *46*, 457–463. [CrossRef] [PubMed]
86. Pawlukojć, A.; Natkaniec, I.; Grech, E.; Baran, J.; Malarski, Z.; Sobczyk, L. Incoherent inelastic neutron scattering, Raman and IR absorption studies on 1,8-bis(dimethylamino)naphthalene and its protonated forms. *Spectrochim. Acta A* **1998**, *54*, 439–448. [CrossRef]
87. Antonov, A.S.; Pozharskii, A.F.; Tolstoy, P.M.; Filarowski, A.; Khoroshilova, O.V. 1,8-Bis(dimethylamino) naphthyl-2-ketimines: Inside vs. outside protonation. *Beilstein J. Org. Chem.* **2018**, *14*, 2940–2948. [CrossRef] [PubMed]
88. Jezierska, A.; Panek, J.J. "Zwitterionic proton sponge" hydrogen bonding investigations on the basis of Car-Parrinello molecular dynamics. *J. Chem. Inf. Model.* **2015**, *55*, 1148–1157. [CrossRef]
89. Ozeryanskii, V.A.; Pozharskii, A.F.; Antonov, A.S.; Filarowski, A. Out-Basicity of 1,8-bis(dimethylamino) naphthalene: The experimental and theoretical challenge. *Org. Biomol. Chem.* **2014**, *12*, 2360–2369. [CrossRef]
90. Pozharskii, A.F.; Degtyarev, A.V.; Ryabtsova, O.V.; Ozeryanskii, V.A.; Kletskii, M.E.; Starikova, Z.A.; Sobczyk, L.; Filarowski, A. 2-α-hydroxyalkyl- and 2,7-di(α-hydroxyalkyl)-1,8-bis(dimethylamino)naphthalenes: Stabilization of nonconventional in/out conformers of "proton sponges" via N···H-O intramolecular hydrogen bonding. A remarkable kind of tandem nitrogen inversion. *J. Org. Chem.* **2007**, *72*, 3006–3019. [CrossRef]
91. Howard, S.T. Conformers, Energetics, and Basicity of 2,2′-Bipyridine. *J. Am. Chem. Soc.* **1996**, *118*, 10269–10274. [CrossRef]
92. Lesnichin, S.B.; Kamdem, N.; Mauder, D.; Denisov, G.S.; Shenderovich, I.G. Studies of Adsorption of 2,2′-Bipyridyl on the Surface of Highly Regulated Silica Matrix of the MCM-41 Type by Means of ^{15}N NMR Spectroscopy. *Russ. J. Gen. Chem.* **2010**, *80*, 2027–2031. [CrossRef]
93. Kühn, F.E.; Groarke, M.; Bencze, E.; Herdtweck, E.; Prazeres, A.; Santos, A.M.; Calhorda, M.J.; Romao, C.C.; Goncalves, I.S.; Lopes, A.D.; et al. Octahedral Bipyridine and Bipyrimidine Dioxomolybdenum(VI) Complexes: Characterization, Application in Catalytic Epoxidation, and Density Functional Mechanistic Study. *Chem. Eur. J.* **2002**, *8*, 2370–2383. [CrossRef]
94. Lavender, E.S.; Glidewell, C.; Ferguson, G. 1,3,5-Trihydroxybenzene-2,2′-Bipyridyl (1/2): A Hydrogen-Bonded Structure Based on a Stem-and-Leaves Motif. *Acta Crystallogr. Sect. C Cryst. Struct. Commun.* **1998**, *54*, 1637–1639. [CrossRef]
95. Vogler, A.; Shenderovich, I.G. Photochemistry of deprotonated rhenium(I) (3,3′-dihydroxy-2,2′-bipyridine) tricarbonyl chloride. Photoisomerization at the chelate in basic solution. *Inorg. Chim. Acta* **2014**, *421*, 496–499. [CrossRef]

96. Morancho, R.; Pouvreau, P.; Constant, G.; Jaud, J.; Galy, J. Synthese et etude structurale d'un nouveau compose du silicium: Di-2,2′-bipyridine silicium. *J. Organomet. Chem.* **1979**, *166*, 329–338. [CrossRef]
97. Barker, D.J.; Summers, L.A.; Cooney, R.P. Conformations of 2,2′-bipyridine in acidic media. *J. Mol. Struct.* **1987**, *159*, 249–254. [CrossRef]
98. Lesnichin, S.B.; Tolstoy, P.M.; Limbach, H.-H.; Shenderovich, I.G. Counteranion-Dependent Mechanisms of Intramolecular Proton Transfer in Aprotic Solution. *Phys. Chem. Chem. Phys.* **2010**, *12*, 10373–10379. [CrossRef]
99. Chan, B.; Del Bene, J.E.; Radom, L. What factors determine whether a proton-bound homodimer has a symmetric or an asymmetric hydrogen bond? *Mol. Phys.* **2009**, *107*, 1095–1105. [CrossRef]
100. Chan, B.; Del Bene, J.E.; Radom, L. Proton-Bound Homodimers: How Are the Binding Energies Related to Proton Affinities? *J. Am. Chem. Soc.* **2007**, *129*, 12197–12199. [CrossRef]
101. Chan, B.; Del Bene, J.E.; Radom, L. Proton-bound homodimers involving second-row atoms. *Theor. Chem. Acc.* **2012**, *131*, 1088. [CrossRef]
102. Grabowski, S.J.; Ugalde, J.M. High-level ab initio calculations on low barrier hydrogen bonds and protonbound homodimers. *Chem. Phys. Lett.* **2010**, *493*, 37–44. [CrossRef]
103. Cotton, C.E.; Francisco, J.S.; Klemperer, W. Computational study of the linear proton bound ion–molecule complexes of $HCNH^+$ with HCN and HNC. *J. Chem. Phys.* **2013**, *139*, 014304. [CrossRef]
104. Denisov, G.S.; Melikova, S.M.; Rutkovskii, K.S.; Tokhadze, K.G. Spectral Diagnostics of the Dynamics of the Formation of a Homoconjugated Complex $[HCN.H.NCH]^+$. *Opt. Spectrosc.* **2020**, *128*, 467–469. [CrossRef]
105. Terrill, K.; Nesbitt, D.J. Ab initio anharmonic vibrational frequency predictions for linear proton-bound complexes $OC–H^+–CO$ and $N_2–H^+–N_2$. *Phys. Chem. Chem. Phys.* **2010**, *12*, 8311–8322. [CrossRef] [PubMed]
106. Fridgen, T.D.; Parnis, J.M. Electron bombardment matrix isolation of Rg/Rg′/methanol mixtures (Rg=Ar, Kr, Xe): Fourier-transform infrared characterization of the proton-bound dimers Kr_2H^+, Xe_2H^+, $(ArHKr)^+$ and $(ArHXe)^+$ in Ar matrices and $(KrHXe)^+$ and Xe_2H^+ in Kr matrices. *J. Chem. Phys.* **1998**, *109*, 2155. [CrossRef]
107. Kunttu, H.; Seetula, J.; Räsänen, M.; Apkarian, V.A. Photogeneration of ions via delocalized charge transfer states. I. Xe_2H^+ and Xe_2D^+ in solid Xe. *J. Chem. Phys.* **1992**, *96*, 5630. [CrossRef]
108. Grabowski, S.J. $[FHF]^-$—The Strongest Hydrogen Bond under the Influence of External Interactions. *Crystals* **2016**, *6*, 3. [CrossRef]
109. Shenderovich, I.G.; Smirnov, S.N.; Denisov, G.S.; Gindin, V.A.; Golubev, N.S.; Dunger, A.; Reibke, R.; Kirpekar, S.; Malkina, O.L.; Limbach, H.-H. Nuclear Magnetic Resonance of Hydrogen Bonded Clusters between F^- and $(HF)_n$: Experiment and Theory. *Ber. Bunsenges. Phys. Chem. Chem. Phys.* **1998**, *102*, 422–428. [CrossRef]
110. Panich, A.M. NMR study of the F-H···F hydrogen bond. Relation between hydrogen atom position and F-H···F bond length. *Chem. Phys.* **1995**, *196*, 511–519. [CrossRef]
111. Fujiwara, F.Y.; Martin, J.S. Heterobihalide ions. Nuclear magnetic resonance spectroscopy of strong hydrogen bonds. *J. Am. Chem. Soc.* **1974**, *96*, 7625–7631. [CrossRef]
112. Wenthold, P.G.; Squires, R.R. Bond Dissociation Energies of F_2 and HF_2^-. *A Gas-Phase Experimental and G2 Theoretical Study. J. Phys. Chem.* **1995**, *99*, 2002–2005. [CrossRef]
113. Yamdagni, R.; Kebarle, P. The Hydrogen Bond Energies in $ClHCl^-$ and Cl-$(HCl)_n$. *Can. J. Chem.* **1974**, *52*, 2449–2453. [CrossRef]
114. Cho, H.-G.; Andrews, L. Matrix Infrared Spectra, Photochemistry and Density Functional Calculations of $Cl^-{-}HCCl_2$, $ClHCl^-$, Cl−ClCCl, and $Cl^-{-}HCHCl$ Produced from $CHCl_3$ and CH_2Cl_2 Exposed to Irradiation from Laser Ablation. *J. Phys. Chem. A* **2019**, *123*, 1051–1061. [CrossRef] [PubMed]
115. Maiorov, V.D.; Sysoeva, S.G.; Temkin, O.N.; Kislina, L.S. IR Study of ion-molecular interactions in a DMF-HCl system. *Russ. Chem. Bull.* **1993**, *42*, 1511–1516. [CrossRef]
116. Shenderovich, I.G.; Tolstoy, P.M.; Golubev, N.S.; Smirnov, S.N.; Denisov, G.S.; Limbach, H.-H. Low-Temperature NMR Studies of the Structure and Dynamics of a Novel Series of Acid-Base Complexes of HF with Collidine Exhibiting Scalar Couplings Across Hydrogen Bonds. *J. Am. Chem. Soc.* **2003**, *125*, 11710–11720. [CrossRef] [PubMed]
117. Pylaeva, S.A.; Elgabarty, H.; Sebastiani, D.; Tolstoy, P.M. Symmetry and dynamics of FHF^- anion in vacuum, in CD_2Cl_2 and in CCl_4. Ab initio MD study of fluctuating solvent–solute hydrogen and halogen bonds. *Phys. Chem. Chem. Phys.* **2017**, *19*, 26107–26120. [CrossRef]
118. Golubev, N.S.; Shenderovich, I.G.; Tolstoy, P.M.; Shchepkin, D.N. Solvent Induced Temperature Dependencies of NMR Parameters of Hydrogen Bonded Anionic Clusters. *J. Molec. Struct.* **2004**, *697*, 9–15. [CrossRef]
119. Tupikina, E.Y.; Tolstoy, P.M.; Titova, A.A.; Kostin, M.A.; Denisov, G.S. Estimations of FH···X hydrogen bond energies from IR intensities: Iogansen's rule revisited. *J. Comput. Chem.* **2021**, *42*, 572–580. [CrossRef] [PubMed]
120. Tupikina, E.Y.; Tokhadze, K.G.; Karpov, V.V.; Denisov, G.S.; Tolstoy, P.M. Stretching force constants as descriptors of energy and geometry of F···HF hydrogen bonds. *Spectrochim. Acta A* **2020**, *241*, 118677. [CrossRef] [PubMed]
121. Tupikina, E.Y.; Denisov, G.S.; Melikova, S.M.; Kucherov, S.Y.; Tolstoy, P.M. New look at the Badger-Bauer rule: Correlations of spectroscopic IR and NMR parameters with hydrogen bond energy and geometry. FHF complexes. *J. Mol. Struct.* **2018**, *1164*, 129–136. [CrossRef]
122. Denisov, G.S.; Bureiko, S.F.; Kucherov, S.Y.; Tolstoy, P.M. Correlation relationships between the energy and spectroscopic parameters of complexes with F···HF hydrogen bond. *Dokl. Phys. Chem.* **2017**, *475*, 115–118. [CrossRef]

123. Del Bene, J.E.; Jordan, M.J.T.; Perera, S.A.; Bartlett, R.J. Vibrational effects on the F-F spin-spin coupling constant ($^{2h}J_{F\text{-}F}$) in FHF^- and FDF^-. *J. Phys. Chem. A* **2001**, *105*, 8399–8402. [CrossRef]
124. Limbach, H.-H.; Pietrzak, M.; Sharif, S.; Tolstoy, P.M.; Shenderovich, I.G.; Smirnov, S.N.; Golubev, N.S.; Denisov, G.S. NMR-Parameters and Geometries of OHN and ODN Hydrogen Bonds of Pyridine-Acid Complexes. *Chem. Eur J.* **2004**, *10*, 5195–5204. [CrossRef] [PubMed]
125. Akcakayiran, D.; Mauder, D.; Hess, C.; Sievers, T.K.; Kurth, D.G.; Shenderovich, I.; Limbach, H.-H.; Findenegg, G.H. Carboxylic Acid-Doped SBA-15 Silica as a Host for Metallo-supramolecular Coordination Polymers. *J. Phys. Chem. B* **2008**, *112*, 14637–14647. [CrossRef]
126. Ip, B.C.K.; Andreeva, D.V.; Buntkowsky, G.; Akcakayiran, D.; Findenegg, G.H.; Shenderovich, I.G. NMR Study of Proton Transfer to Strong Bases on Inner Surfaces of MCM-41. *Micropor. Mesopor. Mater.* **2010**, *134*, 22–28. [CrossRef]
127. Andreeva, D.V.; Ip, B.; Gurinov, A.A.; Tolstoy, P.M.; Denisov, G.S.; Shenderovich, I.G.; Limbach, H.-H. Geometrical Features of Hydrogen Bonded Complexes Involving Sterically Hindered Pyridines. *J. Phys. Chem. A* **2006**, *110*, 10872–10879. [CrossRef]
128. Lorente, P.; Shenderovich, I.G.; Golubev, N.S.; Denisov, G.S.; Buntkowsky, G.; Limbach, H.-H. $^{1}H/^{15}N$ NMR Chemical Shielding, Dipolar $^{15}N,^{2}H$ Coupling and Hydrogen Bond Geometry Correlations in a Novel Serious of Hydrogen-Bonded Acid-Base Complexes of Collidine with Carboxylic Acids. *Magn. Reson. Chem.* **2001**, *39*, S18–S29. [CrossRef]
129. Lesnichin, S.B.; Shenderovich, I.G.; Muljati, T.; Limbach, H.-H.; Silverman, D. Intrinsic Proton Donating Power of Zinc-bound Water in a Carbonic Anhydrase Active Site Model Estimated by NMR. *J. Am. Chem. Soc.* **2011**, *133*, 11331–11338. [CrossRef]
130. Tolstoy, P.M.; Smirnov, S.N.; Shenderovich, I.G.; Golubev, N.S.; Denisov, G.S.; Limbach, H.-H. NMR Studies of Solid State—Solvent and H/D Isotope Effects on Hydrogen Bond Geometries of 1:1 Complexes of Collidine with Carboxylic Acids. *J. Molec. Struct.* **2004**, *700*, 19–27. [CrossRef]
131. Gurinov, A.A.; Rozhkova, Y.A.; Zukal, A.; Čejka, J.; Shenderovich, I.G. Mutable Lewis and Brønsted Acidity of Aluminated SBA-15 as Revealed by NMR of Adsorbed Pyridine-^{15}N. *Langmuir* **2011**, *27*, 12115–12123. [CrossRef]
132. Shenderovich, I.G.; Buntkowsky, G.; Schreiber, A.; Gedat, E.; Sharif, S.; Albrecht, J.; Golubev, N.S.; Findenegg, G.H.; Limbach, H.-H. Pyridine-^{15}N—a Mobile NMR Sensor for Surface Acidity and Surface Defects of Mesoporous Silica. *J. Phys. Chem. B* **2003**, *107*, 11924–11939. [CrossRef]
133. Chan-Huot, M.; Dos, A.; Zander, R.; Sharif, S.; Tolstoy, P.M.; Compton, S.; Fogle, E.; Toney, M.D.; Shenderovich, I.; Denisov, G.S.; et al. NMR Studies of Protonation and Hydrogen Bond States of Internal Aldimines of Pyridoxal 5′-Phosphate Acid−Base in Alanine Racemase, Aspartate Aminotransferase, and Poly-L-lysine. *J. Am. Chem. Soc.* **2013**, *135*, 18160–18175. [CrossRef] [PubMed]
134. Limbach, H.-H.; Chan-Huot, M.; Sharif, S.; Tolstoy, P.M.; Shenderovich, I.G.; Denisov, G.S. Critical Hydrogen Bonds and Protonation States of Pyridoxal 5′-phosphate Revealed by NMR. *Biochim. Biophys. Acta* **2011**, *1814*, 1426–1437. [CrossRef]
135. Ip, B.C.K.; Shenderovich, I.G.; Tolstoy, P.M.; Frydel, J.; Denisov, G.S.; Buntkowsky, G.; Limbach, H.-H. NMR Studies of Solid Pentachlorophenol-4-Methylpyridine Complexes Exhibiting Strong OHN Hydrogen Bonds: Geometric H/D Isotope Effects and Hydrogen Bond Coupling Cause Isotopic Polymorphism. *J. Phys. Chem. A* **2012**, *116*, 11370–11387. [CrossRef] [PubMed]
136. Bismarck, A.; Aranberri-Askargorta, I.; Springer, J.; Lampke, T.; Wielage, B.; Stamboulis, A.; Shenderovich, I.; Limbach, H.-H. Surface Characterization of Flax, Hemp and Cellulose Fibers; Surface Properties and the Water Uptake Behavior. *Polym. Compos.* **2002**, *23*, 872–894. [CrossRef]
137. Gurinov, A.A.; Denisov, G.S.; Borissova, A.O.; Goloveshkin, A.S.; Greindl, J.; Limbach, H.-H.; Shenderovich, I.G. NMR Study of Solvation Effect on the Geometry of Proton-Bound Homodimers of Increasing Size. *J. Phys. Chem. A* **2017**, *121*, 8697–8705. [CrossRef] [PubMed]
138. Attah, I.K.; Platt, S.P.; Meot-Ner, M.; El-Shall, M.S.; Aziz, S.G.; Alyoubi, A.O. Proton-bound dimers of nitrogen heterocyclic molecules: Substituent effects on the structures and binding energies of homodimers of diazine, triazine, and fluoropyridine. *J. Chem. Phys.* **2014**, *140*, 114313. [CrossRef]
139. Pollice, R.; Bot, M.; Kobylianskii, I.J.; Shenderovich, I.; Chen, P. Attenuation of London Dispersion in Dichloromethane Solutions. *J. Am. Chem. Soc.* **2017**, *139*, 13126–13140. [CrossRef] [PubMed]
140. Gurinov, A.A.; Lesnichin, S.B.; Limbach, H.-H.; Shenderovich, I.G. How Short is the Strongest Hydrogen Bond in the Proton-Bound Homodimers of Pyridine Derivatives? *J. Phys. Chem. A* **2014**, *118*, 10804–10812. [CrossRef]
141. Kong, S.; Borissova, A.O.; Lesnichin, S.B.; Hartl, M.; Daemen, L.L.; Eckert, J.; Antipin, M.Y.; Shenderovich, I.G. Geometry and Spectral Properties of the Protonated Homodimer of Pyridine in the Liquid and Solid States. A Combined NMR, X-ray Diffraction and Inelastic Neutron Scattering Study. *J. Phys. Chem. A* **2011**, *115*, 8041–8048. [CrossRef]
142. Shenderovich, I.G. Qualitative analysis of the geometry of the hydrogen bond in the homoconjugated pyridine ion. *Russ. J. Gen. Chem.* **2007**, *77*, 620. [CrossRef]
143. Shenderovich, I.G.; Denisov, G.S. Modeling of Solute–Solvent Interactions Using an External Electric Field—From Tautomeric Equilibrium in Nonpolar Solvents to the Dissociation of Alkali Metal Halides. *Molecules* **2021**, *26*, 1283. [CrossRef]
144. Shenderovich, I.G.; Denisov, G.S. Adduct under Field—A Qualitative Approach to Account for Solvent Effect on Hydrogen Bonding. *Molecules* **2020**, *25*, 436. [CrossRef]
145. Shenderovich, I.G.; Denisov, G.S. Solvent effects on acid-base complexes. What is more important: A macroscopic reaction field or solute-solvent interactions? *J. Chem. Phys.* **2019**, *150*, 204505. [CrossRef]

146. Mori, Y.; Takano, K. Location of protons in N-H···N hydrogen-bonded systems: A theoretical study on intramolecular pyridine-dihydropyridine and pyridine-pyridinium pairs. *Phys. Chem. Chem. Phys.* **2012**, *14*, 11090–11098. [CrossRef]
147. Rozhkova, Y.A.; Gurinov, A.A.; Orlova, A.O.; Maslov, V.G.; Shenderovich, I.G.; Korotkov, V.I. Spectrophotometric investigations of protonated forms of heterocyclic compounds. *Opt. Spectrosc.* **2012**, *113*, 275–278. [CrossRef]
148. Melikova, S.M.; Rutkowski, K.S.; Gurinov, A.A.; Denisov, G.S.; Rospenk, M.; Shenderovich, I.G. FTIR study of the hydrogen bond symmetry in protonated homodimers of pyridine and collidine in solution. *J. Mol. Struct.* **2012**, *1018*, 39–44. [CrossRef]
149. Guzei, I.A.; Roberts, J.; Saulys, D.A. Pseudosymmetry in pyridinium-tetrachloro(oxo)pyridineniobate(V) pyridine solvate. *Acta Crystallogr. Sect. C Cryst. Struct. Commun.* **2002**, *58*, m141–m143. [CrossRef] [PubMed]
150. Katrusiak, A. Stereochemistry and transformations of NH—N hydrogen bonds Part I. Structural preferences for the hydrogen site. *J. Mol. Struct.* **1999**, *474*, 125–133. [CrossRef]
151. Brencic, J.V.; Ceh, B.; Leban, I. Pyridinium tetrabromobis (pyridine)tungstate (III), $[(py)_2H][WBr_4(py)_2]$. *Acta Crystallogr. Sect. B Struct. Crystallogr. Cryst. Chem.* **1979**, *35*, 3028–3030. [CrossRef]
152. Minshall, P.C.; Sheldrick, G.M. Pyridinium 2,2,5,5-tetrathio-cyclo-di(phosphadithianate), $[(pyridine)_2H]_2{}^{2+}[P_2S_8]^{2-}$. *Acta Crystallogr. Sect. B Struct. Crystallogr. Cryst. Chem.* **1978**, *34*, 1378–1380. [CrossRef]
153. Drew, M.G.B.; McKee, V.; Nelson, S.M. Crystal and molecular structure and some properties of pyridinium μ-oxo-bis[trichioroferrate(III)]–pyridine. *J. Chem. Soc. Dalton Trans.* **1978**, 80–84. [CrossRef]
154. Villarreal-Salinas, B.E.; Schlemper, E.O. Crystal structure of a salt of the pyridinium-pyridine ion by X-ray and neutron diffraction. *J. Cryst. Mol. Struct.* **1978**, *8*, 217–237. [CrossRef]
155. Pollice, R.; Fleckenstein, F.; Shenderovich, I.; Chen, P. Compensation of London Dispersion in the Gas Phase and in Aprotic Solvents. *Angew. Chem. Int. Ed.* **2019**, *58*, 14281–14288. [CrossRef] [PubMed]
156. Taft, R.W.; Bordwell, F.G. Structural and solvent effects evaluated from acidities measured in dimethyl sulfoxide and in the gas phase. *Acc. Chem. Res.* **1988**, *21*, 463–469. [CrossRef]
157. Grabowski, S.J. Hydrogen and halogen bonds are ruled by the same mechanisms. *Phys. Chem. Chem. Phys.* **2013**, *15*, 7249–7259. [CrossRef] [PubMed]
158. Grabowski, S.J. QTAIM Characteristics of Halogen Bond and Related Interactions. *J. Phys. Chem. A* **2012**, *116*, 1838–1845. [CrossRef]
159. Nejad, A.; Suhm, M.A. Concerted Pair Motion Due to Double Hydrogen Bonding: The Formic Acid Dimer Case. *J. Indian I. Sci.* **2020**, *100*, 5–19. [CrossRef]
160. Tautermann, C.S.; Loferer, M.J.; Voegele, A.F.; Liedl, K.R. Double hydrogen tunneling revisited: The breakdown of experimental tunneling criteria. *J. Chem. Phys.* **2004**, *120*, 11650. [CrossRef]
161. Emmeluth, C.; Suhm, M.A.; Luckhaus, D. A monomers-in-dimers model for carboxylic acid dimers. *J. Chem. Phys.* **2003**, *118*, 2242–2255. [CrossRef]
162. Vener, M.V.; Kühn, O.; Bowman, J.M. Vibrational spectrum of the formic acid dimer in the OH stretch region. A model 3D study. *Chem. Phys. Lett.* **2001**, *349*, 562–570. [CrossRef]
163. Elsaesser, T.; Huse, N.; Dreyer, J.; Dwyer, J.R.; Heyne, K.; Nibbering, E.T.J. Ultrafast vibrational dynamics and anharmonic couplings of hydrogen-bonded dimers in solution. *Chem. Phys.* **2007**, *341*, 175–188. [CrossRef]
164. Tolstoy, P.M.; Schah-Mohammedi, P.; Smirnov, S.N.; Golubev, N.S.; Denisov, G.S.; Limbach, H.-H. Characterization of Fluxional Hydrogen-Bonded Complexes of Acetic Acid and Acetate by NMR: Geometries and Isotope and Solvent Effects. *J. Am. Chem. Soc.* **2004**, *126*, 5621–5634. [CrossRef] [PubMed]
165. Wu, G.; Hung, I.; Gan, Z.; Terskikh, V.; Kong, X. Solid-State ^{17}O NMR Study of Carboxylic Acid Dimers: Simultaneously Accessing Spectral Properties of Low- and High-Energy Tautomers. *J. Phys. Chem. A* **2019**, *123*, 8243–8253. [CrossRef]
166. Grabowski, S.J. What Is the Covalency of Hydrogen Bonding? *Chem. Rev.* **2011**, *111*, 2597–2625. [CrossRef]
167. Davies, J.A.; Hanson-Heine, M.W.D.; Besley, N.A.; Shirley, A.; Trowers, J.; Yang, S.; Ellis, A.M. Dimers of acetic acid in helium nanodroplets. *Phys. Chem. Chem. Phys.* **2019**, *21*, 13950–13958. [CrossRef] [PubMed]
168. Manriquez, R.; Lopez-Dellamary, F.A.; Frydel, J.; Emmler, T.; Breitzke, H.; Buntkowsky, G.; Limbach, H.-H.; Shenderovich, I.G. Solid-State NMR Studies of Aminocarboxylic Salt Bridges in L-Lysine Modified Cellulose. *J. Phys. Chem. B* **2009**, *113*, 934–940. [CrossRef] [PubMed]
169. Golubev, N.S.; Smirnov, S.N.; Schah-Mohammedi, P.; Shenderovich, I.; Denisov, G.S.; Gindin, V.; Limbach, H.-H. Study of Acid-Base Interaction by Means of Low-Temperature NMR Spectra. Structure of Salicilic Acid Complexes. *Russ. J. Gen. Chem.* **1997**, *67*, 1082–1087.
170. Jing Guo, J.; Tolstoy, P.M.; Koeppe, B.; Golubev, N.S.; Denisov, G.S.; Smirnov, S.N.; Limbach, H.-H. Hydrogen Bond Geometries and Proton Tautomerism of Homoconjugated Anions of Carboxylic Acids Studied via H/D Isotope Effects on ^{13}C NMR Chemical Shifts. *J. Phys. Chem. A* **2012**, *116*, 11180–11188. [CrossRef]
171. Reiersølmoen, A.C.; Battaglia, S.; Øien-Ødegaard, S.; Gupta, A.K.; Fiksdahl, A.; Lindh, R.; Erdélyi, M. Symmetry of three-center, four-electron bonds. *Chem. Sci.* **2020**, *11*, 7979. [CrossRef]
172. Hakkert, S.B.; Erdélyi, M. Halogen bond symmetry: The N–X–N bond. *J. Phys. Org. Chem.* **2015**, *28*, 226–233. [CrossRef]
173. Karim, A.; Reitti, M.; Carlsson, A.-C.C.; Gräfenstein, J.; Erdélyi, M. The nature of $[N–Cl–N]^+$ and $[N–F–N]^+$ halogen bonds in solution. *Chem. Sci.* **2014**, *5*, 3226–3233. [CrossRef]

174. Carlsson, A.-C.C.; Gräfenstein, J.; Budnjo, A.; Laurila, J.L.; Bergquist, J.; Karim, A.; Kleinmaier, R.; Brath, U.; Erdélyi, M. Symmetric Halogen Bonding Is Preferred in Solution. *J. Am. Chem. Soc.* **2012**, *134*, 5706–5715. [CrossRef]
175. Troyanov, S.I.; Morozov, I.V.; Kemnitz, E. Crystal Structure of Cesium Dihydrotrifluoride, CsH_2F_3. Refinement of the Crystal Structures of NMe_4HF_2 and $NMe_4H_2F_3$. *Z. Anorg. Allg. Chem.* **2005**, *631*, 1651–1654. [CrossRef]
176. Tian, C.; Nie, W.; Chen, Q.; Sun, G.; Borzov, M.V. Modified approach to the Arduengo carbene complexes of silver. *Russ. Chem. Bull.* **2014**, *63*, 2675–2680. [CrossRef]
177. Mootz, D.; Boenigk, D. Poly(hydrogen Fluorides) with the Tetramethylammonium Cation: Preparation, Stability Ranges, Crystal Structures, $[H_nF_{n+1}]^-$ Anion Homology, Hydrogen Bonding F-H ... F. *Z. Anorg. Allg. Chem.* **1987**, *544*, 159–166. [CrossRef]
178. Fernández, F.J.; Alfonso, M.; Schmalle, H.W.; Berke, H. Utilization of Redox and Acid/Base Chemistry for the Deprotection of a $Mn(dmpe)_2(\dot{C}CSiMe_3)_2$ Complex. *Organometallics* **2001**, *20*, 3122–3131. [CrossRef]
179. Forrester, J.D.; Senko, M.E.; Zalkin, A.; Templeton, D. Crystal structure of KH_2F_3 and geometry of the $H_2F_3^-$ ion. *Acta Cryst.* **1963**, *16*, 58–62. [CrossRef]
180. Wilson, W.W.; Chxiste, K.O.; Feng, J.; Bau, R. Tetramethylammonium bifluoride, crystal structure and vibrational spectra. *Can. J. Chem.* **1989**, *67*, 1898–1901. [CrossRef]
181. Freza, S.; Skurski, P. Enormously large (approaching 14 eV!) electron binding energies of $[H_nF_{n+1}]^-$ (n = 1–5, 7, 9, 12) anions. *Chem. Phys. Lett.* **2010**, *487*, 19–23. [CrossRef]
182. Schneider, H.-J. Hydrogen bonds with fluorine. Studies in solution, in gas phase and by computations, conflicting conclusions from crystallographic analyses. *Chem. Sci.* **2012**, *3*, 1381–1394. [CrossRef]
183. Bulychev, V.P.; Buturlimova, M.V. Anharmonic calculation of structural and vibrational properties of the isolated complexes $[F(HF)_2]^-$, $[F(DF)_2]^-$, and $[F(TF)_2]^-$. *J. Mol. Struct.* **2009**, *928*, 32–39. [CrossRef]
184. Bulychev, V.P.; Denisov, G.S.; Limbach, H.-H.; Shukailov, R.M. Calculation of vibrations of the H-bonds and electrooptical parameters of the $[F(HF)_2]^-$ complex. *Opt. Spectrosc.* **2001**, *90*, 356–361. [CrossRef]
185. de la Vega, G.J.M.; Fabian, S.J. Assessment of DFT functionals with fluorine-fluorine coupling constants. *Mol. Phys.* **2015**, *113*, 1924–1936. [CrossRef]
186. Alkorta, I.; Elguero, J.; Limbach, H.-H.; Shenderovich, I.G.; Winkler, T. A DFT and AIM Analysis of the Spin-Spin Couplings Across the Hydrogen Bond in the 2-fluorobenzamide and Related Compounds. *Magn. Reson. Chem.* **2009**, *47*, 585–592. [CrossRef] [PubMed]
187. Del Bene, J.E.; Alkorta, I.; Elguero, J. A Systematic Comparison of Second-Order Polarization Propagator Approximation (SOPPA) and Equation-of-Motion Coupled Cluster Singles and Doubles (EOM-CCSD) Spin-Spin Coupling Constants for Selected Singly Bonded Molecules, and the Hydrides NH_3, H_2O, and HF and Their Protonated and Deprotonated Ions and Hydrogen-Bonded Complexes. *J. Chem. Theory Comput.* **2008**, *4*, 967–973. [CrossRef]
188. Del Bene, J.E.; Elguero, J. ^{19}F–^{19}F and ^{19}F–^{1}H spin–spin coupling constants in cyclic FH polymers $(FH)_n$, n = 2–6. *Solid State Nucl. Magn. Reson.* **2008**, *34*, 86–92. [CrossRef] [PubMed]
189. Del Bene, J.E.; Elguero, J.; Alkorta, I.; Yanez, M.; Mo, O. ^{19}F-^{19}F spin-spin coupling constant surfaces for $(HF)_2$ clusters: The orientation and distance dependence of the sign and magnitude of J(F-F). *J. Chem. Phys.* **2004**, *120*, 3237–3243. [CrossRef]
190. Del Bene, J.E.; Alkorta, I.; Elguero, J. Computed EOM-CCSD ^{19}F-^{19}F spin-spin coupling constants in small organic molecules. *Z. Phys. Chem.* **2003**, *217*, 1565–1575. [CrossRef]
191. Perera, S.A.; Bartlett, R.J. NMR spin-spin coupling constants for hydrogen bonds of $[F(HF)_n]^-$, n=1-4, clusters. *J. Am. Chem. Soc.* **2000**, *122*, 1231–1232. [CrossRef]
192. Golubev, N.S.; Shenderovich, I.G.; Smirnov, S.N.; Denisov, G.S.; Limbach, H.-H. Nuclear Scalar Spin-Spin Coupling Reveals Novel Properties of Low-Barrier Hydrogen Bonds in a Polar Environment. *Chem. Eur. J.* **1999**, *5*, 492–497. [CrossRef]
193. Tupikina, E.Y.; Denisov, G.S.; Tolstoy, P.M. Anticooperativity of FH···Cl$^-$ hydrogen bonds in $[FH)_nCl]^-$ clusters (n = 1 ... 6). *J. Comput. Chem.* **2019**, *40*, 2858–2867. [CrossRef] [PubMed]
194. Kucherov, S.Y.; Bureiko, S.F.; Denisov, G.S. Anticooperativity of FHF hydrogen bonds in clusters of the type $F^-\times(HF)_n$, $RF\times(HF)_n$ and $XF\times(HF)_n$, R = alkyl and X = H, Br, Cl, F. *J. Mol. Struct.* **2016**, *1105*, 246–255. [CrossRef]
195. Grabowski, S.J. Cooperativity of hydrogen and halogen bond interactions. *Theor. Chem. Acc.* **2013**, *132*, 1347. [CrossRef]
196. Ziółkowski, M.; Grabowski, S.J.; Leszczynski, J. Cooperativity in Hydrogen-Bonded Interactions: Ab Initio and "Atoms in Molecules" Analyses. *J. Phys. Chem. A* **2006**, *110*, 6514–6521. [CrossRef]
197. Shenderovich, I.G.; Lesnichin, S.B.; Tu, C.; Silverman, D.N.; Tolstoy, P.M.; Denisov, G.S.; Limbach, H.-H. NMR Studies of Active-Site Properties of Human Carbonic Anhydrase II by using ^{15}N-Labeled 4-Methylimidazole as a Local Probe and Histidine Hydrogen-Bond Correlations. *Chem. Eur. J.* **2015**, *21*, 2915–2929. [CrossRef]
198. Sharif, S.; Fogle, E.; Toney, M.D.; Denisov, G.S.; Shenderovich, I.G.; Buntkowsky, G.; Tolstoy, P.M.; Chan Huot, M.; Limbach, H.-H. NMR Localization of Protons in Critical Enzyme Hydrogen Bonds. *J. Am. Chem. Soc.* **2007**, *129*, 9558–9559. [CrossRef]
199. Mulloyarova, V.V.; Giba, I.S.; Kostin, M.A.; Denisov, G.S.; Shenderovich, I.G.; Tolstoy, P.M. Cyclic Trimers of Phosphinic Acids in Polar Aprotic Solvent: Symmetry, Chirality and H/D Isotope Effects on NMR Chemical Shifts. *Phys. Chem. Chem. Phys.* **2018**, *20*, 4901–4910. [CrossRef]
200. Shenderovich, I.G. The Partner Does Matter: The Structure of Heteroaggregates of Acridine Orange in Water. *Molecules* **2019**, *24*, 2816. [CrossRef]

201. Gurinov, A.A.; Mauder, D.; Akcakayiran, D.; Findenegg, G.H.; Shenderovich, I.G. Does Water Affect the Acidity of Surfaces? The Proton-Donating Ability of Silanol and Carboxylic Acid Groups at Mesoporous Silica. *ChemPhysChem* **2012**, *13*, 2282–2285. [CrossRef]
202. Mauder, D.; Akcakayiran, D.; Lesnichin, S.B.; Findenegg, G.H.; Shenderovich, I.G. Acidity of Sulfonic and Phosphonic Acid-Functionalized SBA-15 under Almost Water-Free Conditions. *J. Phys. Chem. C* **2009**, *113*, 19185–19192. [CrossRef]
203. Shenderovich, I.G.; Limbach, H.-H.; Smirnov, S.N.; Tolstoy, P.M.; Denisov, G.S.; Golubev, N.S. H/D Isotope Effects on the Low-Temperature NMR Parameters and Hydrogen Bond Geometries of $(FH)_2F^-$ and $(FH)_3F^-$ Dissolved in CDF_3/CDF_2Cl. *Phys. Chem. Chem. Phys.* **2002**, *4*, 5488–5497. [CrossRef]
204. Mulloyarova, V.V.; Ustimchuk, D.O.; Filarowski, A.; Tolstoy, P.M. H/D Isotope Effects on ^{1}H-NMR Chemical Shifts in Cyclic Heterodimers and Heterotrimers of Phosphinic and Phosphoric Acids. *Molecules* **2020**, *25*, 1907. [CrossRef]
205. Machida, S.; Sohmiya, M.; Ide, Y.; Sugahara, Y. Solid-State ^{31}P Nuclear Magnetic Resonance Study of Interlayer Hydroxide Surfaces of Kaolinite Probed with an Interlayer Triethylphosphine Oxide Monolayer. *Langmuir* **2018**, *34*, 12694–12701. [CrossRef]
206. Seitz, A.E.; Hippauf, F.; Kremer, W.; Kaskel, S.; Scheer, M. Facile storage and release of white phosphorus and yellow arsenic. *Nat. Commun.* **2018**, *9*, 361. [CrossRef] [PubMed]
207. Moussa, M.E.; Shelyganov, P.A.; Wegley, B.; Seidl, M.; Scheer, M. The Potential of the Diphosphorus Complex $[Cp_2W_2(CO)_4(\eta^2\text{-}P_2)]$ as an Organometallic Connecter in Supramolecular Chemistry. *Eur. J. Inorg. Chem.* **2019**, *2019*, 4241–4248. [CrossRef]
208. Guenther, J.; Reibenspies, J.; Blümel, J. Synthesis and characterization of tridentate phosphine ligands incorporating long methylene chains and ethoxysilane groups for immobilizing molecular rhodium catalysts. *Mol. Catal.* **2019**, *479*, 110629. [CrossRef]
209. Cluff, K.J.; Bhuvanesh, N.; Blümel, J. Monometallic Ni-0 and Heterobimetallic Ni-0/Au-I Complexes of Tripodal Phosphine Ligands: Characterization in Solution and in the Solid State and Catalysis. *Chem. Eur. J.* **2015**, *21*, 10138–10148. [CrossRef]
210. Pazderski, L. ^{15}N and ^{31}P NMR Coordination Shifts in Transition Metal Complexes with Nitrogen- and Phosphorus-Containing Heterocycles. *Annu. Rep. NMR Spectrosc.* **2013**, *80*, 33–179. [CrossRef]
211. Hubbard, P.J.; Benzie, J.W.; Bakhmutov, V.I.; Blümel, J. Disentangling Different Modes of Mobility of Triphenylphosphine Oxide Adsorbed on Alumina. *J. Chem. Phys.* **2020**, *152*, 054718. [CrossRef]
212. Kharel, S.; Cluff, K.J.; Bhuvanesh, N.; Gladysz, J.A.; Blümel, J. Structures and Dynamics of Secondary and Tertiary Alkylphosphine Oxides Adsorbed on Silica. *Chem. Asian J.* **2019**, *14*, 2704–2711. [CrossRef]
213. Hilliard, C.R.; Kharel, S.; Cluff, K.; Bhuvanesh, N.; Gladysz, J.; Bluemel, J. Structures and Unexpected Dynamic Properties of Phosphine Oxides Adsorbed on Silica Surfaces. *Chem. Eur. J.* **2014**, *20*, 17292–17295. [CrossRef]
214. Shenderovich, I.G. For Whom a Puddle Is the Sea? Adsorption of Organic Guests on Hydrated MCM-41 Silica. *Langmuir* **2020**, *36*, 11383–11392. [CrossRef] [PubMed]
215. Shenderovich, I.G. Effect of Noncovalent Interactions on the ^{31}P Chemical Shift Tensor of Phosphine Oxides, Phosphinic, Phosphonic, and Phosphoric Acids, and Their Complexes with Lead(II). *J. Phys. Chem. C* **2013**, *117*, 26689–26702. [CrossRef]
216. Shenderovich, I.G. Electric field effect on 31P NMR magnetic shielding. *J. Chem. Phys.* **2020**, *153*, 184501. [CrossRef] [PubMed]
217. Chernyshov, I.Y.; Vener, M.V.; Shenderovich, I.G. Local-structure effects on ^{31}P NMR chemical shift tensors in solid state. *J. Chem. Phys.* **2019**, *150*, 144706. [CrossRef]
218. Fisher, K.J.; Alyea, E.C.; Shehnazarian, N. A ^{31}P NMR Study of the Water Soluble Derivatives of 1,3,5-triaza-7-phosphaadamantane (PTA). *Phosphorus Sulfur Silicon* **1990**, *48*, 37–40. [CrossRef]
219. Phillips, A.D.; Gonsalvi, L.; Romerosa, A.; Vizza, F.; Peruzzini, M. Coordination chemistry of 1,3,5-triaza-7-phosphaadamantane (PTA) Transition metal complexes and related catalytic, medicinal and photoluminescent applications. *Coord. Chem. Rev.* **2004**, *248*, 955–993. [CrossRef]
220. Battistin, F.; Balducci, G.; Milani, B.; Alessio, E. Water-Soluble Ruthenium(II) Carbonyls with 1,3,5-Triaza-7-phosphoadamantane. *Inorg. Chem.* **2018**, *57*, 6991–7005. [CrossRef]
221. Battistin, F.; Balducci, G.; Iengo, E.; Demitri, N.; Alessio, E. Neutral 1,3,5-Triaza-7-phosphaadamantane-Ruthenium(II) Complexes as Precursors for the Preparation of Highly Water-Soluble Derivatives. *Eur. J. Inorg. Chem.* **2016**, *2016*, 2850–2860. [CrossRef]
222. Frisch, M.J.; Trucks, G.W.; Schlegel, H.B.; Scuseria, G.E.; Robb, M.A.; Cheeseman, J.R.; Scalmani, G.; Barone, V.; Mennucci, B.; Petersson, G.A.; et al. *Gaussian 09, Revision D.01*; Gaussian, Inc.: Wallingford, CT, USA, 2013.
223. Chai, J.-D.; Head-Gordon, M. Long-range corrected hybrid density functionals with damped atom-atom dispersion corrections. *Phys. Chem. Chem. Phys.* **2008**, *10*, 6615–6620. [CrossRef] [PubMed]
224. Weigend, F.; Ahlrichs, R. Balanced basis sets of split valence, triple zeta valence and quadruple zeta valence quality for H to Rn: Design and assessment of accuracy. *Phys. Chem. Chem. Phys.* **2005**, *7*, 3297–3305. [CrossRef] [PubMed]
225. Alyea, E.C.; Ferguson, G.; Kannan, S. Intermolecular hydrogen···metal interactions. The crystal structure of {cis-$[PdCl_2(TPA)_2]\}_2\cdot H_2O$, a water-soluble palladium (II) tertiary phosphine complex. *Chem. Commun.* **1998**, 345–346. [CrossRef]
226. Otto, S.; Roodt, A.; Purcell, W. Synthesis and characterisation of water soluble Pt(II) complexes of 1,3,5-triaza-7-phosphaadamantane (PTA). Crystal and molecular structure of {*cis*-$[PtCl_2(PTA)2]\}_2\cdot H_2O$. *Inorg. Chem. Commun.* **1998**, *1*, 415–417. [CrossRef]
227. Braddock-Wilking, J.; Acharya, S.; Rath, N.P. Synthesis and characterization of Pt(II) and Pd(II) PTA and DAPTA complexes. *Polyhedron* **2014**, *79*, 16–28. [CrossRef]
228. Shenderovich, I.G. Experimentally Established Benchmark Calculations of ^{31}P NMR Quantities. *Chem. Methods* **2021**, *1*, 61–70. [CrossRef]

229. Darensbourg, D.J.; Robertson, J.B.; Larkins, D.L.; Reibenspies, J.H. Water-Soluble Organometallic Compounds. 7.1 Further Studies of 1,3,5-Triaza-7-Phosphaadamantane Derivatives of Group 10 Metals, Including Metal Carbonyls and Hydrides. *Inorg. Chem.* **1999**, *38*, 2473–2481. [CrossRef]
230. Darensbourg, D.J.; Decuir, T.J.; Stafford, N.W.; Robertson, J.B.; Draper, J.D.; Reibenspies, J.H. Water-Soluble Organometallic Compounds. 6.1 Synthesis, Spectral Properties, and Crystal Structures of Complexes of 1,3,5-Triaza-7-phosphaadamantane with Group 10 Metals. *Inorg. Chem.* **1997**, *36*, 4218–4226. [CrossRef]
231. Kirillov, A.M.; Smoleński, P.; Guedes da Silva, M.F.C.; Pombeiro, A.J.L. The First Copper Complexes Bearing the 1,3,5-Triaza-7-phosphaadamantane (PTA) Ligand. *Eur. J. Inorg. Chem.* **2007**, *2007*, 2686–2692. [CrossRef]
232. Alyea, E.C.; Ferguson, G.; Kannan, S. Some water-soluble organometallic complexes of group 10 transition metal(II) ions with 1,3,5-triaza-7-phosphaadamantane (TPA). Syntheses, characterization and reactivity. The crystal and molecular structure of $[Ni(CN)_2(TPA)_3]\cdot 4.3H_2O$. *Polyhedron* **1998**, *17*, 2727–2732. [CrossRef]
233. Grünberg, B.; Emmler, T.; Gedat, E.; Shenderovich, I.; Findenegg, G.H.; Limbach, H.-H.; Buntkowsky, G. Hydrogen Bonding of Water Confined in Mesoporous Silica MCM-41 and SBA-15 Studied by ^{1}H Solid-State NMR. *Chem. Eur. J.* **2004**, *10*, 5689–5696. [CrossRef]
234. Buntkowsky, G.; Breitzke, H.; Adamczyk, A.; Roelofs, F.; Emmler, T.; Gedat, E.; Grünberg, B.; Xu, Y.; Limbach, H.-H.; Shenderovich, I.; et al. Structural and Dynamical Properties of Guest Molecules Confined in Mesoporous Silica Materials Revealed by NMR. *Phys. Chem. Chem. Phys.* **2007**, *9*, 4843–4853. [CrossRef]
235. Gedat, E.; Schreiber, A.; Findenegg, G.H.; Shenderovich, I.; Limbach, H.-H.; Buntkowsky, G. Stray Field Gradient NMR Reveals Effects of Hydrogen Bonding on Diffusion Coefficients of Pyridine in Mesoporous Silica. *Magn. Reson. Chem.* **2001**, *39*, S149–S157. [CrossRef]
236. Masaru, N.; Chihiro, W. Monomeric and Cluster States of Water Molecules in Organic Solvent. *Chem. Lett.* **1992**, *21*, 809–812. [CrossRef]
237. Sharif, S.; Shenderovich, I.G.; González, L.; Denisov, G.S.; Silverman, D.N.; Limbach, H.-H. NMR and Ab initio Studies of Small Complexes Formed between Water and Pyridine Derivatives in Solid and Liquid Phase. *J. Phys. Chem. A* **2007**, *111*, 6084–6093. [CrossRef]
238. Baures, P.W. Monoclinic Triphenylphosphine Oxide Hemihydrate. *Acta Crystallogr. Sect. C Cryst. Struct. Commun.* **1991**, *47*, 2715–2716. [CrossRef]
239. Ng, S.W. A Second Monoclinic Modification of Triphenylphosphine Oxide Hemihydrate. *Acta Crystallogr. Sect. E Struct. Rep. Online* **2009**, *65*, o1431. [CrossRef]
240. Begimova, G.U.; Tupikina, E.Y.; Yu, V.K.; Denisov, G.S.; Bodensteiner, M.; Shenderovich, I.G. Effect of Hydrogen Bonding to Water on the ^{31}P Chemical Shift Tensor of Phenyl- and Trialkylphosphine Oxides and a-Amino Phosphonates. *J. Phys. Chem. C* **2016**, *120*, 8717–8729. [CrossRef]
241. Tupikina, E.Y.; Bodensteiner, M.; Tolstoy, P.M.; Denisov, G.S.; Shenderovich, I.G. P=O Moiety as an Ambidextrous Hydrogen Bond Acceptor. *J. Phys. Chem. C* **2018**, *122*, 1711–1720. [CrossRef]
242. Hilliard, C.R.; Bhuvanesh, N.; Gladysz, J.A.; Blümel, J. Synthesis, purification, and characterization of phosphine oxides and their hydrogen peroxide adducts. *Dalton Trans.* **2012**, *41*, 1742–1754. [CrossRef]
243. Ahn, S.H.; Cluff, K.J.; Bhuvanesh, N.; Blümel, J. Hydrogen Peroxide and Di(hydroperoxy)propane Adducts of Phosphine Oxides as Stoichiometric and Soluble Oxidizing Agents. *Angew. Chem. Int. Ed.* **2015**, *54*, 13341–13345. [CrossRef]
244. Arp, F.F.; Bhuvanesh, N.; Blümel, J. Hydrogen peroxide adducts of triarylphosphine oxides. *Dalton Trans.* **2019**, *48*, 14312–14325. [CrossRef]
245. Forlani, L. Hydrogen bonds of anilines. In *The Chemistry Anilines*; Rappoport, Z., Ed.; The Atrium, Southern Gate, West Sussex PO19 8SQ, Part 1; John Wiley & Sons Ltd.: Chichester, UK, 2007; pp. 407–454.
246. Szatyłowicz, H.; Krygowski, T.M.; Hobza, P. How the Shape of the NH_2 Group Depends on the Substituent Effect and H-Bond Formation in Derivatives of Aniline. *J. Phys. Chem. A* **2007**, *111*, 170–175. [CrossRef]
247. Borisenko, V.E.; Filarovski, A.I. The electrooptical parameters of aniline and its halogen derivatives in hydrogen bonded complexes. *J. Mol. Struct.* **1989**, *196*, 353–370. [CrossRef]
248. Grabowski, S.J. Pnicogen and tetrel bonds—tetrahedral Lewis acid centres. *Struct. Chem.* **2019**, *30*, 1141–1152. [CrossRef]
249. Grabowski, S.J. Triel bond and coordination of triel centres—Comparison with hydrogen bond interaction. *Coord. Chem. Rev.* **2020**, *407*, 213171. [CrossRef]
250. Pelties, S.; Maier, T.; Herrmann, D.; de Bruin, B.; Rebreyend, C.; Gärtner, S.; Shenderovich, I.G.; Wolf, R. Selective P4 Activation by a Highly Reduced Cobaltate: Synthesis of Dicobalt Tetraphosphido Complexes. *Chem. Eur. J.* **2017**, *23*, 6094–6102. [CrossRef]
251. Maier, T.M.; Sandl, S.; Shenderovich, I.G.; von Wangelin, A.J.; Weigand, J.J.; Wolf, R. Amine-Borane Dehydrogenation and Transfer Hydrogenation Catalyzed by alpha-Diimine Cobaltates. *Chem. Eur. J.* **2019**, *25*, 238–245. [CrossRef]
252. Medvedev, A.G.; Churakov, A.V.; Prikhodchenko, P.V.; Lev, O.; Vener, M.V. Crystalline Peroxosolvates: Nature of the Coformer, Hydrogen-Bonded Networks and Clusters, Intermolecular Interactions. *Molecules* **2021**, *26*, 26. [CrossRef] [PubMed]
253. Giba, I.S.; Tolstoy, P.M. Self-Assembly of Hydrogen-Bonded Cage Tetramers of Phosphonic Acid. *Symmetry* **2021**, *13*, 258. [CrossRef]

254. Kizior, B.; Panek, J.J.; Szyja, B.M.; Jezierska, A. Structure-Property Relationship in Selected Naphtho- and Anthra-Quinone Derivatives on the Basis of Density Functional Theory and Car–Parrinello Molecular Dynamics. *Symmetry* **2021**, *13*, 564. [CrossRef]
255. Alkorta, I.; Elguero, J.; Frontera, A. Not Only Hydrogen Bonds: Other Noncovalent Interactions. *Crystals* **2020**, *10*, 180. [CrossRef]